AGU PUBLICATIONS

JGR

Journal of Geophysical Research: Space Physics

RESEARCH ARTICLE
10.1002/2017JA024216

Special Section:
Observations, Simulations, and Theory of Electric Currents in the Solar System

Key Points:
- Thin and intense current layers with a half-thickness L of ~30–100 km $\leq \rho_{H+}$ embedded in a thicker CSs are observed in the Martian magnetotail
- The embedded current layers can be explained by quasi-adiabatic dynamics of multicomponent ion population
- The CS thickness depends on B_N/B_0 and on V_T/V_D of the dominant ion component in agreement with the quasi-adiabatic scaling law

Correspondence to:
E. E. Grigorenko,
elenagrigorenko2003@yandex.ru

Citation:
Grigorenko, E. E., Shuvalov, S. D., Malova, H. V., Dubinin, E., Popov, V. Y., Zelenyi, L. M., … McFadden, J. P. (2017). Imprints of quasi-adiabatic ion dynamics on the current sheet structures observed in the Martian magnetotail by MAVEN. *Journal of Geophysical Research: Space Physics*, *122*. https://doi.org/10.1002/2017JA024216

Received 31 MAR 2017
Accepted 13 SEP 2017
Accepted article online 18 SEP 2017

Imprints of Quasi-Adiabatic Ion Dynamics on the Current Sheet Structures Observed in the Martian Magnetotail by MAVEN

E. E. Grigorenko[1,2], S. D. Shuvalov[1], H. V. Malova[1,3], E. Dubinin[4], V. Yu. Popov[1,5,6], L. M. Zelenyi[1], J. Espley[7], and J. P. McFadden[8]

[1]Space Research Institute of RAS, Moscow, Russia, [2]Moscow Institute of Physics and Technology, Moscow, Russia, [3]Scobeltsyn Nuclear Physics Institute, Lomonosov Moscow State University, Moscow, Russia, [4]Max Planck Institute for Solar System Research, Göttingen, Germany, [5]Physics Department, Lomonosov Moscow State University, Moscow, Russia, [6]Higher School of Economics, National University, Moscow, Russia, [7]NASA Goddard Space Flight Center, Greenbelt, MD, USA, [8]Space Sciences Laboratory University of California, Berkeley, CA, USA

Abstract Numerous studies of the current sheets (CS) in the Earth's magnetotail showed that quasi-adiabatic ion dynamics plays an important role in the formation of complicated multilayered current structures. In order to check whether the similar mechanisms operate in the Martian magnetotail, we analyzed 80 CS crossings using MAVEN measurements on the nightside of Mars at radial distances ~1.0–2.8R_M. We found that CS structures experience similar dependence on the value of the normal component of the magnetic field at the neutral plane (B_N) and on the ratio of the ion drift velocity outside the CS to the thermal velocity (V_T/V_D) as it was observed for the CSs in the Earth's magnetotail. For the small values of B_N, a thin and intense CS embedded in a thicker one is observed. The half-thickness L of this layer is ~30–100 km $\leq \rho_{H+}$ (ρ_{H+} is a gyroradius of thermal protons outside the CS). With the increase of B_N, the L also increases up to several hundred kilometers (~ρ_{O+}, ρ_{O2+}), the current density decreases, and the embedding feature disappears. Our statistical analysis showed a good agreement between L values observed by MAVEN and the CS scaling obtained from the quasi-adiabatic model, if the plasma characteristics in Martian CSs are used as input parameters. Thus, we may conclude that in spite of the differences in magnetic topology, ion composition, and plasma thermal characteristics observed in the Earth's and Martian magnetotails, similar quasi-adiabatic mechanisms contribute to the formation of the CSs in the magnetotails of both planets.

1. Introduction

Current sheets (CSs) are the important objects in space plasma as they separate the regions with different magnetic characteristics (e.g., the regions of opposite polarity of the magnetic field), accumulating magnetic energy and releasing it via magnetic reconnection. Thus, it is not surprising that the problem of CS self-organization and stability is one of the key problems in space plasma physics.

Numerous observations of the CSs in the Earth's magnetotail provide much information on their spatial structure and evolution (e.g., Baumjohann et al., 2007, 2010, and references therein). It was revealed that very often the structure of the CS significantly differs from the simple isotropic Harris CS model (Harris, 1962). Multipoint Cluster observations demonstrated that the spatial profiles of the current density along the normal (N) to the CS plane often exhibit complicated multilayered structure in which a thin and intense current layer is embedded in a thicker layer(s) having a smaller current density (e.g., Petrukovich et al., 2011). Typical thickness of a thin current layer in the Earth's magnetotail was of the order or less than the proton thermal gyroradius. It is known now that the thin CSs are the sources of magnetic reconnection (e.g., Asano et al., 2003; Baumjohann, Paschmann, & Nagai, 1992; Runov et al., 2008) because of their metastability (Zelenyi et al., 2008). Thin CSs are often observed in the Earth's and planetary magnetospheres (e.g., Baumjohann et al., 2010; Bunce, Cowley, & Wild, 2003; Uritsky et al., 2015; Vasko et al., 2014; Zelenyi et al., 2016). Recently, STEREO observations were used to show that strong and thin CSs are also observed in the solar wind (e.g., Malova et al., 2017).

These observations stimulated the development of many theoretical models of thin CSs. The analytical isotropic models in which magnetic tension of curved field lines is balanced by the radial plasma

pressure gradient (Kan, 1973; Shindler, 1974; Birn, 1987) have been exploited in magnetosphere physics for a long time. In pioneer papers by Speiser (1965) and Eastwood (1972), another possibility to balance the tension of magnetic field lines by centrifugal force exerted on ions moving along curved magnetic field lines was suggested. Such model of the CS balance implies the existence of the finite plasma anisotropy outside the CS. Contrary to the isotropic CS, a thin CS has the extent along the directions tangential to the sheet plane much larger than the extent along the normal to the CS plane. In such thin CSs, the magnetic field tension is balanced by the anisotropy of plasma pressure tensor. This consideration was based on the existence of the so-called Speiser particles that experience quasi-adiabatic dynamics in the CS.

Particles become quasi-adiabatic when their maximal gyroradius ρ_{max}, usually achieved at the neutral plane of the CS, is larger than the radius of curvature of the magnetic field lines, R. Such particles become unmagnetized near the neutral plane of the CS and experience a complicated motion consisting of fast oscillations along the normal to the CS plane and slow quasi-Larmor gyration in the CS plane around a finite normal component of the magnetic field (B_N). The magnetic moment μ of such particles is not conserved, but in the quasi-adiabatic regime when $R < \rho_{max}$, there is another integral of particle motion $I_N = (2\pi)^{-1} \oint p_N dN \approx \text{const}$ (here, N is the direction of particle fast oscillations and p_N is a particle momentum in that direction). The conservation of I_N is possible with the parameter of adiabaticity $\kappa = (R/\rho_{max})^{1/2} < 1.0$ (Büchner & Zelenyi, 1989). The dynamics of such particles is called "quasi-adiabatic" because the I_N is conserved, although the magnetic moment μ is not conserved. If $\kappa = 1.0$, then neither the I_N nor μ are conserved and particle motion becomes chaotic. Such particles experience the nonadiabatic dynamics.

The quasi-adiabatic particles, also called "Speiser particles," can carry the significant current in a thin CS. The motion of Speiser particles is almost "regular" everywhere except the localized separatrix regions at which the I_N experiences jumps, and the type of particle motion transforms from magnetized to an unmagnetized one and vice versa, that is, at the entrance and exit from the CS. The value of total variation of I_N (the sum of jumps) defines the type of orbit the particle has in the CS. Generally, $\Delta I_N \neq 0$, and particles experience scattering and can be partially or fully trapped within the CS. The fully trapped plasma particles moving along closed trajectories do not produce the net electric current in the CS but affect its structure making the CS thicker. The quasi-trapped population experiences multiple interactions with the CS and further chaotization and finally supplements the trapped population. This process leads to the "aging" of the CS and to the growth of its thickness (Zelenyi et al., 2002). For some special conditions, the I_N jumps are fully compensated, so that $\Delta I_N = 0$ and the particles are ejected from the CS after the interaction almost without scattering and move along open Speiser trajectories (e.g., Grigorenko et al., 2011, and references therein). Such particles produce the strongest net current in the CS.

The peculiarities of particle interactions with the CS and the partition between Speiser-type, quasi-trapped and trapped plasma populations lead to the evolution of the CS spatial structure and influence its stability. Usually in a thin CS, electrons are completely magnetized ($\kappa >> 1.0$), while ions can experience quasi-adiabatic interactions with the CS ($\kappa < 1.0$; e.g., Ashour-Abdalla et al., 1994). In such CSs, the dynamics of ions and electrons is very different and should be considered separately. This stimulates the development of hybrid models, in which electrons are considered as fluid, while ion dynamics is described in the frames of kinetic approach (e.g., Sitnov et al., 2000; Zelenyi et al., 2000, 2004).

Because the jumps of quasi-adiabatic integral of motion ΔI_N depend on the κ parameter, which, in turn, depends on ion gyroradius, then in the one and the same initial magnetic configuration of the CS, ion populations with different masses and/or temperatures carry different net currents, which are characterized by different spatial scales and values of current density. The kinetic features of quasi-adiabatic ion dynamics in the CSs are responsible for the variety of the current density profiles: bifurcated, embedded, and/or asymmetrical ones. Such current structures are often observed in the Earth's magnetotail and in the solar wind CS (e.g., Baumjohann et al., 2007; Grigorenko et al., 2013, 2015; Malova et al., 2017; Nakamura et al., 2006; Petrukovich et al., 2011; Runov et al., 2003).

The formation of thin and multilayered CSs can be explained in the frames of an analytical self-consistent model of anisotropic CS (Zelenyi et al., 2000). This theory shows that in the close vicinity of the magnetic

field reversal, the paramagnetic current arising from the meandering motion of Speiser ions (Speiser, 1965) dominates. In a case of weak anisotropy of the initial ion distribution ($\varepsilon = V_T/V_D < 1.0$, where V_T is the ion thermal velocity and V_D is the ion drift velocity outside the CS), the maximum thickness of the CS is of the order of the thermal ion gyroradius outside the sheet. Generally, the CS scaling is controlled either by the quasi-adiabatic regimes of weak and strong anisotropy of the initial distribution or, in case of very strong anisotropy, by its nonadiabatic limit. The last corresponds to the case of almost field-aligned initial distribution in which $V_T/V_D < B_N/B_0$ (B_0 is the magnetic field value outside the CS and B_N is the magnetic field component perpendicular to the CS plane and observed at the neutral plane). In this regime, the CS thickness becomes very small and depends on the value of B_N/B_0.

In multicomponent plasma, the dynamics of different ion species having different masses and often different temperatures may significantly affects the structure of the CS. Zelenyi et al. (2006) considered a self-consistent equilibrium model of 1D anisotropic CS with a small finite B_N. In their model, the electron population was taken into account with the assumption of Boltzman-like quasi-equilibrium distribution of the electrostatic electric field, which can lead to the generation of a very thin and intense current layer in the neutral plane of the CS. The inclusion of heavy ion (O^+) population into the model results in the CS broadening due to the formation of "O^+ current wings" at the edges of a thin current layer. Thus, the presence of multicomponent plasma affects the CS structure and can be responsible for the formation of the complicated system of multiple embedded current layers. Similar conditions can occur in the Martian magnetotail.

Unlike the Earth, Mars has no strong internal magnetic field so that the solar wind and interplanetary magnetic field (IMF) interact directly with the planetary ionosphere and form the induced magnetosphere (e.g., Luhmann & Brace, 1991, and references therein; Nagy et al., 2004; Fedorov et al., 2008; Bertucci et al., 2011). This interaction has a complicated character because of the existence of crustal magnetic fields covering the majority of planetary surface with the most intense fields located in the southern hemisphere near 180° longitude (e.g., Acuña et al., 1998; Connerney et al., 2005; Luhmann et al., 2015).

The induced Martian magnetotail is formed by the draping of the IMF around Mars (see, e.g., reviews by Nagy et al., 2004; Crider et al., 2004, and references therein). Early observations by Mars-2, -3, and -5 and Phobos-2 showed that the Martian tail is purely induced and resembles tails of comets and Venus (e.g., Dubinin et al., 1991; Vaisberg, 1992; Yeroshenko et al., 1990). Later, it was shown that the draping of the Martian tail is less than that of the Venus tail (Luhmann et al., 1991) and the tail flaring is controlled by upstream solar wind pressure similar to the dynamics of the Earth's magnetosphere (Zhang et al., 1994). The other similarities between Martian and the Earth's magnetotails include the existence of two magnetic lobes with the enhanced sunward and antisunward fields separated by the CS. The orientation of the Martian lobe magnetic field and the spatial extent of the magnetotail are controlled by the IMF direction (e.g., Romanelli et al., 2015; Yeroshenko et al., 1990).

The cross-tail Martian CS and the surrounding plasma sheet consist of escaping planetary ions accelerated up to a few keV/q (e.g., Barabash et al., 2007; Carlsson et al., 2006; Dubinin et al., 1991, 1993, 2006, 2011; Fedorov et al., 2006; Lundin et al., 1989, 1990; Luhmann et al., 1991; Lundin & Barabash, 2004; Yeroshenko et al., 1990). The distinct feature of the CS ion composition is the abundance of hot heavy ions (e.g., Fedorov et al., 2006; Lundin et al., 2006). These ions make an important contribution to the plasma pressure in the CS and can affect the CS configuration.

The observations of the CSs in the induced Martian magnetotail at different distances from the planet were reported in many studies based on data from different missions (e.g., Acuña et al., 1999; Dubinin et al., 1991; Dubinin & Fraenz, 2015; DiBraccio et al., 2015; Ferguson et al., 2005; Halekas et al., 2006; Harada et al., 2015a, 2015b; Luhmann et al., 1991). It was shown that the dynamics of the Martian CS exhibits many features peculiar to the Earth's magnetotail CS: flapping motions (e.g., Dubinin et al., 2012; DiBraccio et al., 2015, 2017), magnetic reconnection (Eastwood et al., 2008; Halekas et al., 2009; Harada et al., 2015a) and associated plasma flow acceleration (Harada et al., 2015b), and plasmoids formation (DiBraccio et al., 2015; Hara et al., 2017).

A diversity of plasma characteristics in the Martian CS manifests in a wide range of estimated half-thicknesses (L) from $L \leq 100$ km (e.g., Halekas et al., 2006) to a few hundreds of kilometeres (e.g.

Harada et al., 2015a, 2015b). The comparison of the CS half-thickness with particle thermal gyroradius and inertial length allowed Harada et al. (2015a) to conclude that in a thin CS, protons and/or electrons carry the electric current, while in a thick CS, the role of quasi-adiabatic heavy ions (O^+) becomes important.

With the presence of unmagnetized ions ($\kappa < 1.0$) in the CSs of the Martian magnetotail, one may expect that quasi-adiabatic ion dynamics can affect their structure by the similar way as it is observed in the CS of the terrestrial magnetotail. In this paper we verify the validity of the quasi-adiabatic model of anisotropic CS for the description of the CS structures in the Martian magnetotail. For this purpose, on the basis of Mars Atmosphere and Volatile Evolution (MAVEN) spacecraft (Jakosky et al., 2015) observations in the near-Mars tail, we study the spatial structure of the CSs and its dependence on the magnetic configuration of the sheets, namely, on the value of the local normal component of the magnetic field, B_N, at the neutral plane and on the ion characteristics in the CSs. We check the validity of the CS scaling predicted by the self-consistent model of anisotropic CS and whether the observed spatial profiles of the electric current density can be described by the quasi-adiabatic model developed for the Earth's magnetotail CS if the plasma characteristics in Martian CSs are used as input parameters. This study allows to conclude whether the similar quasi-adiabatic mechanisms contribute to the formation of the CSs in the magnetotails of both planets.

2. Observations

For the analysis of magnetic and plasma structure of the CS, we used the magnetic field data from magnetometer (MAG; Connerney et al., 2014) and ion data from Suprathermal and Thermal Ion Composition (STATIC; McFadden et al., 2014) both onboard MAVEN. Our database includes 80 CS crossings observed by MAVEN at $-2.8R_M \le X_{MSO} \le -1.0R_M$ and $-1.0R_M \le Y_{MSO} \le 1.0R_M$. The observations are presented in Mars solar orbital (MSO) coordinates unless noted otherwise: the X_{MSO} is directed from the center of the planet toward the Sun, Z_{MSO} is perpendicular to the Mars orbital plane and is directed northward, and Y_{MSO} completes the right-handed system.

In this study we concentrate on the analysis of the cross-tail CS that separates two lobes of antiparallel magnetic field of the Martian magnetotail formed by the draped IMF (e.g., Luhmann et al., 1991). The crossings of the cross-tail CS are identified by the changes of the polarity of B_X field along with the decrease of $|B|$ and the increase of ion β (e.g., DiBraccio et al., 2015; Dubinin & Fraenz, 2015; Harada et al., 2015a, 2015b).

We analyzed MAVEN observations in the Martian magnetotail during December 2014 and during the first half of April 2015. For the analysis of the CSs, we used the minimum variance analysis (MVA). The MVA method is widely used in space physics for the analysis of CSs, shock fronts, plane waves, and other planar structures. The basic assumption of this method is that the time series of the analyzed data contains a planar and quasi-stationary structure (a current layer), which is crossed by the spacecraft. The details of this method can be found in Sönnerup and Scheible (1998). Under the assumption of 1D current structure, this method allows the determination of the local coordinate system, in which one axis is directed along the direction of minimum magnetic field variation, that is, along the normal to the planar current layer (N); another axis is directed along the maximum magnetic field variation (L), and the third one completes the orthogonal system and is directed along the electric current (M) in the CS.

To analyze the spatial structure of the CSs, we selected only the intervals of full CS crossings, when the magnetic field component along the direction of maximum variance B_L monotonically changes from its positive/negative value in one lobe to the negative/positive value in the opposite lobe. In other words, the sign of dB_L/dt should not change during the CS crossing. Another important condition of the CS selection is the obtaining of well-determined local coordinate system by applying the MVA to the CS crossings: the ratios of intermediate-to-minimum λ_M/λ_N and maximum-to-intermediate λ_L/λ_M eigenvalues should exceed 6.0 Finally, we selected 80 intervals of the CS crossings listed in Table A1 in Appendix A1. Figure 1 shows the MAVEN orbits containing the intervals of the CS crossings from our database (shown by red color).

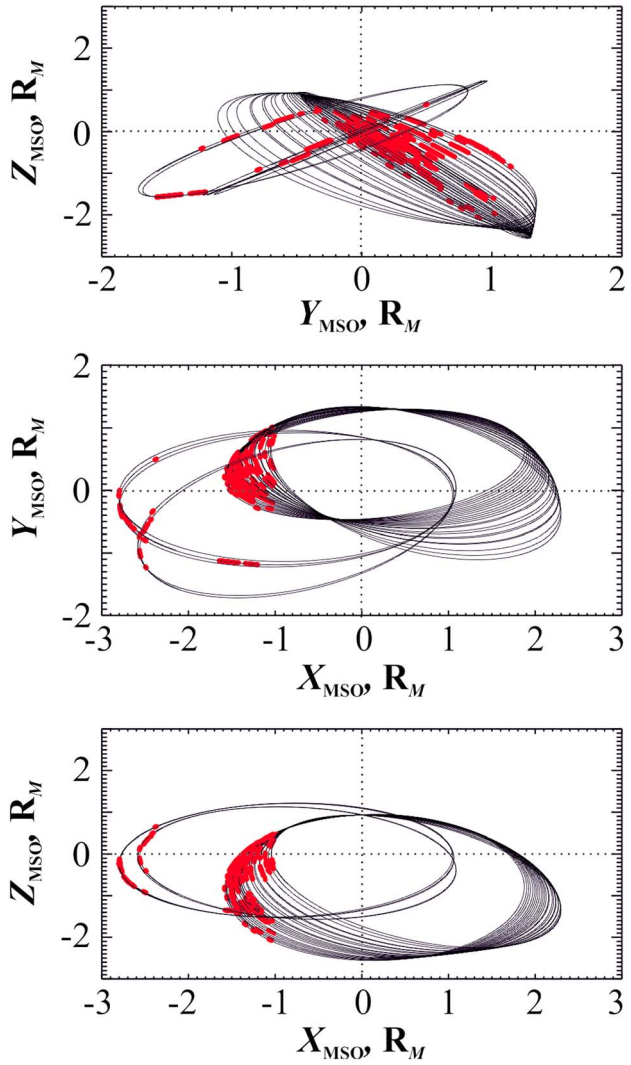

Figure 1. The intervals of MAVEN orbits corresponding to the CS crossings from our database plotted in the $(YZ)_{MSO}$, $(XY)_{MSO}$, and $(XZ)_{MSO}$ planes.

2.1. Observations of a Thin Embedded CS in the Martian Magnetotail

On 4 December 2014 between 14:40 and 14:55, UT MAVEN was located at $[-1.5, 0.5, -1.1]_{MSO}$, and around 14:49 UT, it crossed the CS. This manifests in the reversal of the B_X component from +10 to −8 nT. Figure 2 displays energy–time spectrograms of the main ion components: H^+, O^+, O_2^+, and CO_2^+ (panels a–d), three components of the magnetic field (e), ion densities (h), and temperatures (i). Ions moved mainly tailward with $V_X \sim -10$–15 km/s (not shown). In this CS, crossing heavy ions dominated as is evident in the ratios: $n_{H+}/n_{O+} = 0.1$, $n_{H+}/n_{O2+} = 0.08$, and $n_{H+}/n_{CO2+} = 0.4$ near the neutral plane of the CS. The ratios of proton-to-heavy ion temperatures were as follows: $T_H/T_O = 0.7$, $T_H/T_{O2} = 1.0$, and $T_H/T_{CO2} = 1.0$. The ratio of the ion thermal pressure to the magnetic pressure is $\beta_{ION} = 70.0$ near the neutral plane. The ion pressure was calculated by taking into account H^+ and heavy ion components: $P_{ION} = k\cdot(n_H T_H + n_O T_O + n_{O2} T_{O2} + n_{CO2} T_{CO2})$, k is the Boltzmann constant and n and T are the density and temperature of a given ion component, respectively.

To analyze the CS structure, we used the MVA technique and apply it to the time interval of the B_X reversal indicated by the vertical dashed lines in Figure 2. We defined the normal direction **N** to the CS in the CS-oriented coordinate system (L, M, N), where L indicates the maximum, M intermediate, and N minimum variance directions (e.g., Sönnerup & Scheible, 1998). For this crossing, the MVA directions are almost along the $\mathbf{X}_{MSO}$, $\mathbf{Y}_{MSO}$, and $\mathbf{Z}_{MSO}$ axes (**L** = $[0.9, -0.2, 0.3]_{MSO}$; **M** = $[0.3, 0.9, -0.4]_{MSO}$, and **N** = $[-0.2, 0.45, 0.9]_{MSO}$); the ratios of eigenvalues are $\lambda_M/\lambda_N = 7.5$ and $\lambda_L/\lambda_M = 10.0$. Three MVA components of the magnetic field are shown in Figure 2g. Unfortunately, we cannot define the parameters of the upstream IMF for this CS crossing and make the conclusion on the origin of this CS orientation.

For the Earth's magnetotail, it was shown that the motion of the CS magnetic flux tubes due to flapping or large-scale perturbations causes the corresponding motion of the surrounding plasma. This plasma moves with the normal velocity V_N roughly proportional to the value of the dB_L/dt observed in the course of the CS crossing; that is, the V_N has the same sign during a single crossing (e.g., Sergeev et al., 2003, and references therein). Assuming the planar 1D and quasi-steady current structure, one can estimate the spatial scale of the region of magnetic field reversal, that is, the CS thickness, and reconstruct the spatial distribution of electric current density across the CS.

In the present study, we apply the similar analysis to the CSs observed in the Martian magnetotail. The current density J_M measured at the moment t_i within the sheet should be proportional to $\Delta B_L^i/\Delta I_N^i$, where $\Delta B_L^i = B_L^{i+1} - B_L^i$, $\Delta I_N^i = t_i V_N$ and V_N is the component of plasma bulk velocity along **N**. Because plasma in the Martian magnetotail is multicomponent under the V_N, we consider the corresponding component of the bulk velocity of the center of mass:

$$V_N = (m_H\cdot n_H\cdot V_{N\_H} + m_O\cdot n_O\cdot V_{N\_O} + m_{O2}\cdot n_{O2}\cdot V_{N\_O2} + m_{CO2}\cdot n_{CO2}\cdot V_{N\_CO2})/(m_H\cdot n_H + m_O\cdot n_O + m_{O2}\cdot n_{O2} + m_{CO2}\cdot n_{CO2}).$$

The ion bulk velocities were corrected for the spacecraft velocity. Figure 2f shows the time profiles of the V_N (solid gray line) and V_M components of ion velocities (shown by the colored dotted lines). It is seen that during the time interval of the B_L reversal, the V_N is almost constant. We should note that outside this time interval, the presented values of V_N and V_M can be unreliable, because they were calculated in the local CS coordinate system obtained from the MVA analysis applied to the interval of B_X reversal (indicated by the dashed vertical lines in Figure 2). For the estimation of the CS spatial scale, we used the value of V_N averaged for this time interval.

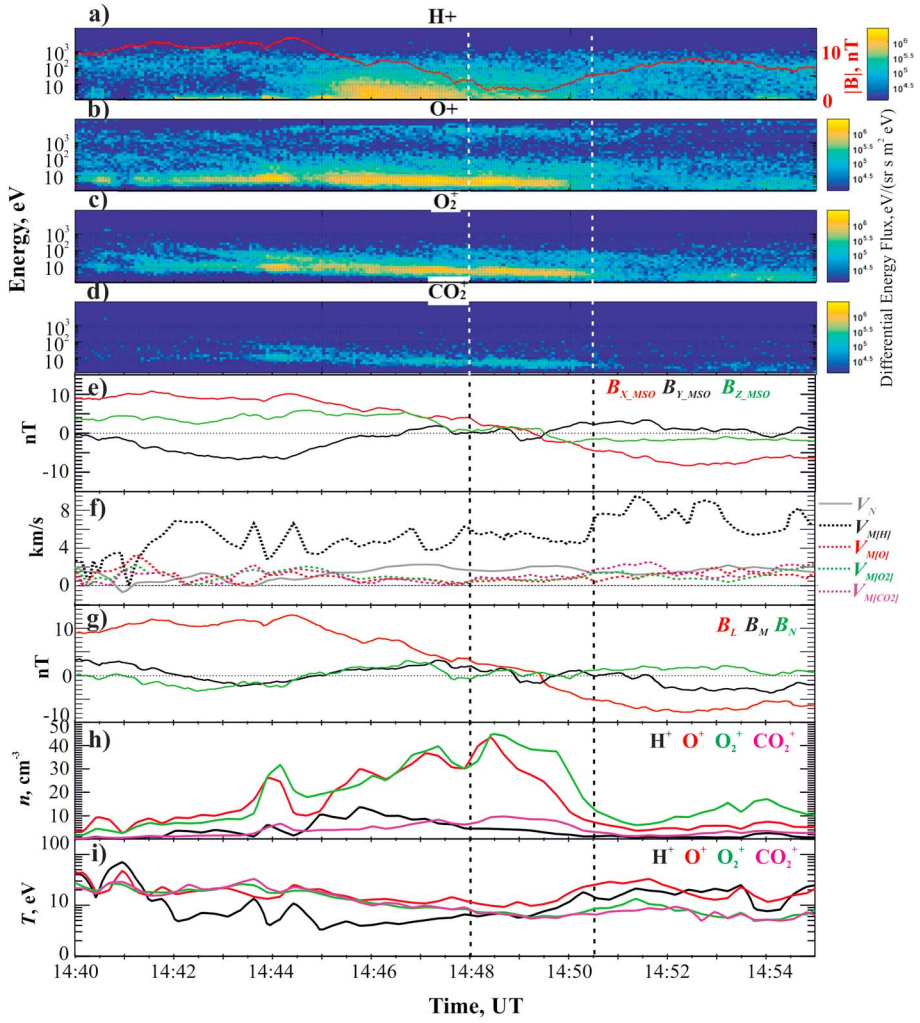

Figure 2. An example of the CS crossing by MAVEN on 4 December 2014. From top to bottom: (a–d) Energy–time spectrograms of omnidirectional H^+, O^+, O_2^+, and CO_2^+ ions; (e) three components of the magnetic field in the MSO coordinate system; (f) time profiles of the normal component velocity of the plasma sheet center mass, V_N (solid gray line), and intermediate component of velocity V_M of the major ion components (shown by the colored dotted lines) calculated from the MVA analysis applied to the time interval of the magnetic field reversal indicated by vertical dashed lines; (g) time profiles of three MVA components of the magnetic field; (h) time profiles of number density of H^+ (black line), O^+ (red line), O_2^+ (green line), and CO_2^+ (magenta line) ion components; (i) time profiles of temperature of H^+, O^+, O_2^+, and CO_2^+ ion components shown by the same colors as in panel (h). The time profile of the absolute value of the magnetic field |**B**| is shown by the red line in panel (a).

To construct the spatial profiles of $B_M(l_N)$ and $J_M(l_N)$, we smoothed magnetic field data by the 4 s sliding average. The total thickness of the CS Λ, that is, the spatial scale of the sheet along the **N** direction, can be estimated as $\Lambda = \int_{t1}^{t2} V_N dt$, where $\Delta t = t_2 - t_1$ is the timescale of the B_L reversal. The spatial profiles of the $B_L(l_N)$ and $J_M(l_N)$ thus obtained are presented in the left column of Figure 3 at plots (a) and (b), respectively.

Such a method of reconstruction of the $J_M(l_N)$ spatial profile was used in a number of previous studies dedicated to the Earth's magnetotail CS (e.g., Petrukovich et al., 2011; Zelenyi et al., 2011). Unfortunately, by using only one-point observations, it is difficult to assess whether the small-scale oscillations of J_M represent temporal or spatial changes. We note that during the CS crossings analyzed in this paper, the strong magnetic fluctuations were absent according to our selection criterion. Thus, we may assume that the reconstructed spatial profile $J_M(l_N)$ more or less reflects the real spatial structure of the CS.

It is seen from the Figure 3a that the slope of $B_L(l_N)$ changes and becomes much steeper at the immediate vicinity of the center of the CS (l_N = 0; this region is shaded by pink color). This feature denotes the

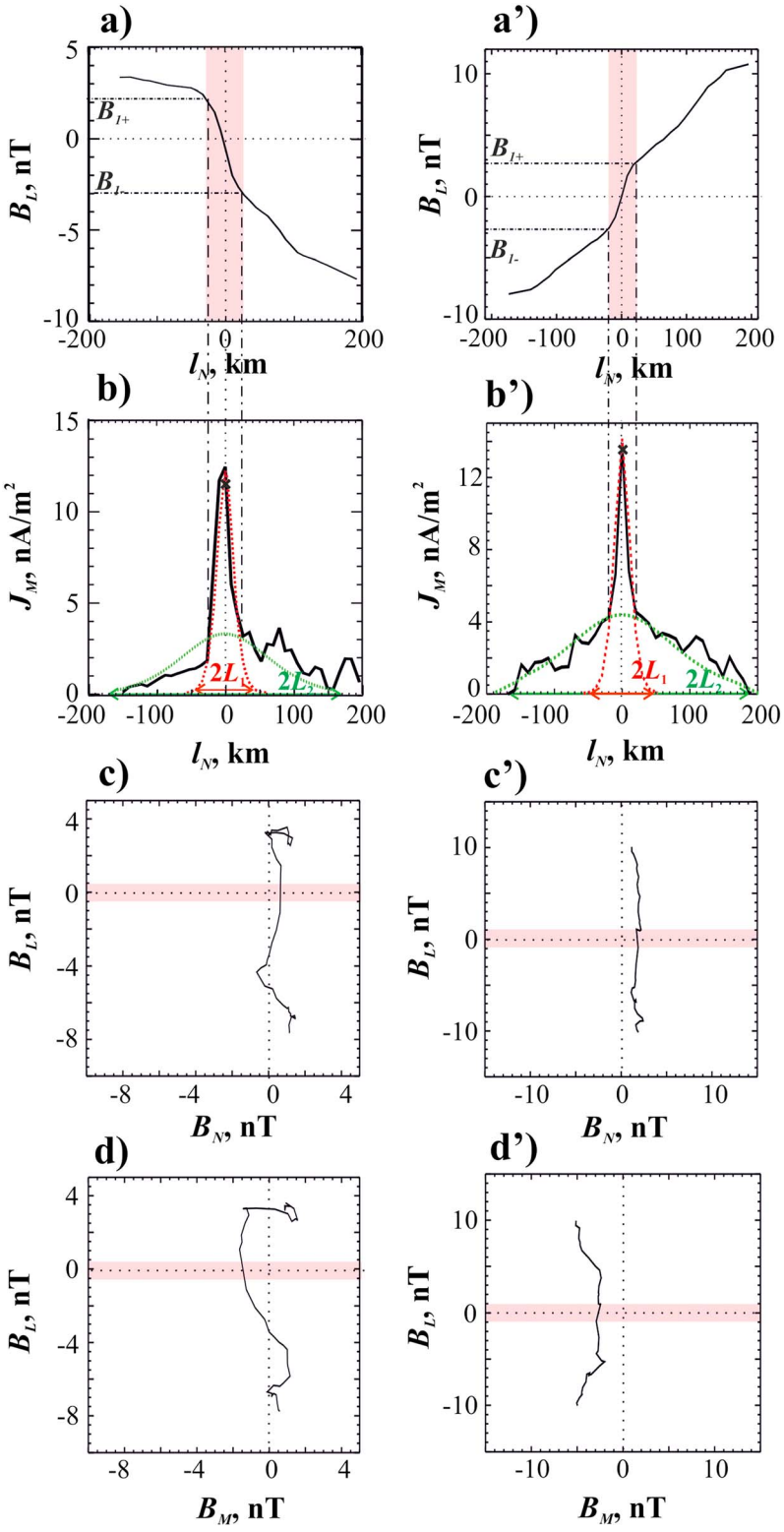

Figure 3. The analysis of the CS structures observed on 4 December 2014 between 14:48:00 and 14:50:30 UT (panels a–d) and on 18 December 2014 between 18:18:28 and 18:18:30 UT (panels a′–d′). From top to bottom: (a, a′) The spatial profile of the $B_L(l_N)$ along the normal direction N to the CS plane; (b, b′) the spatial profile of the electric current density $J_M(l_N)$; (c, c′ and d, d′) the hodograms of the magnetic field in the (B_N, B_L) and (B_M, B_L) planes, respectively, shown for two examples of the CS crossings. In plots (b, b′), the black cross marks the value of the total ion current density calculated at the neutral plane (see explanation in the text).

existence of a stronger electric current near the center of the CS, which is embedded in a thicker current layer with a smaller current density at the CS's periphery. The thick layer is not exactly symmetrical relative to the neutral plane possibly because of some temporal changes in its structure. To illustrate the presence of two current layers in Figure 3b, we show the fitting of the observed current density profile $J_M(l_N)$ by two Harris solutions: $J_{Mi}(l_N) = J_{0i}/\cosh^2(l_N/L_i)$ (Harris, 1962; Petrukovich et al., 2011), where index $i = 1, 2$ corresponds to two current layers: (1) a thin one embedded in (2) a thicker one, which are characterized by the maximum values of the current density at the center ($l_N = 0$): $J_{01} = 12$ nA/m^2 and $J_{02} = 3$ nA/m^2 and by the half-thickness $L_1 = 30$ km and $L_2 = 150$ km, respectively.

Petrukovich et al. (2011) introduced a quantitative parameter to describe the embedding: the ratio of the value of magnetic field at the edges of a thin current layer (B_1) to the value of the magnetic field outside the CS (B_0). The embedding feature exists in the CS when $B_1/B_0 < 1.0$, and it is disappearing while the value of B_1 is approaching to B_0, that is, when $B_1/B_0 = 1.0$. Using the fitting of the observed CS profile by two Harris current layers, one can define the B_1 from the spatial profile of $B_L(l_N)|_{lN = lN^*}$, where l_{N^*} is the coordinate of the intersection of two Harris-type current density profiles. If there is some asymmetry in the observed spatial profile of the $B_L(l_N)$; namely, the value of B_{1+} in the region of positive l_N is not equal to the value of B_{1-} in the region of negative l_N (see Figure 3b,b′), then we estimate the B_1 as an average of these two values: $B_1 = (B_{1+} + B_{1-})/2.0$. For this CS crossing, the parameter of embedding $B_1/B_0 = 0.25$ ($B_1 = 2.5$ nT; see Figure 3a).

The half-thickness of the thin CS is comparable with the gyroradius of thermal protons outside the CS ($\rho_{H+} = 38$ km, calculated for the absolute value of the magnetic field outside the CS $B_0 = 10$ nT and $T_{H+} = 7$ eV) and much smaller than the proton inertial length ($\lambda_p = c/\Omega_H = 743$ km, where c is the speed of light and Ω_H is proton gyrofrequency). The half-thickness of the thicker current layer is of the order of the thermal gyroradius of O^+ ions outside the CS ($\rho_{O+} = 175$ km, calculated for the same B_0 value and for $T_{O+} = 10$ eV). It is worth to note that if, instead of the bulk velocity of the plasma center of mass V_N, one uses the normal component of the spacecraft velocity, assuming that the CS is crossed only due to the spacecraft motion, then all aforementioned features of the current density profile, e.g., the embedding, remain the same, but the estimated half-thickness L will be even smaller: ~20 km for a thin embedded CS and ~100 km for a thicker layer.

Figure 3c,d shows the hodograms of the magnetic field in the (B_N, B_L) and (B_M, B_L) planes, respectively. It is seen that at the neural plane ($B_L = 0$, shaded by pink color), the $B_N = 1.0$ and the intermediate-variance component $B_M = 2.5$ nT, so that $B_N/B_0 = 0.1$, $B_M/B_0 = 0.25$, where $B_0 = 10$ nT is the absolute value of the magnetic field outside the CS. Thus, a shear component of the magnetic field is small in this CS crossing.

To check the presence of quasi-adiabatic particles in the CS, we calculate the parameter of adiabaticity κ for the thermal ion populations. In section 1, we discussed the importance of this parameter in definition of the regime—adiabatic/nonadiabatic/quasi-adiabatic—of particle dynamics in the CS (Büchner & Zelenyi, 1989). If $\kappa >> 1.0$, particles are fully magnetized in the CS. If $\kappa = 1.0$, particles become nonadiabatic and experience strong scattering in the CS. For such particles, the magnetic moment is not conserved nor is the quasi-adiabatic integral of motion I_N. The motion of such particles is chaotic, and they do not contribute to the electric current density in the CS. The most important regime for the CS structuring is the quasi-adiabatic one, which is realized when $\kappa < 1.0$. As it was discussed in section 1, the motion of quasi-adiabatic particles in the CS can be described by the quasi-adiabatic integral I_N. The peculiarities of quasi-adiabatic particle interactions with the CS leads to the appearance of Speiser (transient), quasi-trapped, and trapped plasma populations whose dynamics affect the CS spatial structure. Thus, it is important to know the value of parameter κ for the CS ion populations. The precise calculation of κ is possible when one can calculate the radius of curvature of the magnetic field line crossing the neutral plane of the CS at the site of particle interaction. Using only one-spacecraft observations, it is impossible to perform such calculation. Thus, to compute the κ, we use an alternative method derived from the parabolic magnetic field model of the CS (Büchner & Zelenyi, 1989): $\kappa = \frac{B_{CS}}{B_0}\sqrt{\frac{L}{\rho}}$ where B_{CS} is the minimum absolute value of the magnetic field near the neutral plane of the CS, B_0 is the magnetic field outside the CS, L is the half-thickness of the CS, and ρ is a particle's gyroradius at the minimum magnetic field in the CS. The parameters B_{CS}, B_0, and L can be obtained from observations and from the reconstruction of the current density spatial profile. Thus, κ is a function of particle gyroradius, and for a given magnetic configuration of the CS, the κ depends only on particle energy.

For two current layers observed in this event, we have L_1 = 30 km (for the thin layer), L_2 = 150 km (for the thicker layer), B_{CS} = 2.7 nT and B_0 = 10 nT. For both current layers, we obtain the parameter $\kappa < 1.0$ for all thermal ion components. Because all thermal ion populations experience quasi-adiabatic dynamics in the CS, one could assume that they can provide the main contribution to the electric current in the CS. Indeed, the comparison of the total ion current density $J_{M\_ION} = q \cdot (n_{H+}V_{M\_H+} + n_{O+}V_{M\_O+} + n_{O2+}V_{M\_O2+} + n_{CO2+}V_{M\_CO2+})$ calculated at the neutral plane (marked by a black cross in Figure 3b) shows a good agreement with the maximum value of current density deduced from the magnetic field observations, J_{M_MF}. This means that quasi-adiabatic ions provide the major contribution to the electric current in the CS. Unfortunately, because the STATIC observations have lower time resolution than the magnetic field data, we cannot compare the total spatial profile of the ion current density with the spatial profile of the current density calculated from the magnetic field data.

In the right column of Figure 3, another example of the embedded CS structure is presented in the same format as the one shown in the left column of the Figure. This CS crossing was observed on 18 December 2014 at 18:28:00–18:30:30 UT. The B_X component of the magnetic field changes its sign as it increases from −8 to 10 nT. During the crossing MAVEN was located at the Martian magnetotail at $[-1.2, 0.3, 0.0]_{MSO}$. The MVA analysis applied to this interval provided well determined local coordinate system with $\mathbf{L} = [0.0, -0.1, 0.98]_{MSO}$; $\mathbf{M} = [0.1, 0.98, 0.1]_{MSO}$; and $\mathbf{N} = [0.0, -0.1, 0.98]_{MSO}$; the ratios of eigenvalues $\lambda_M/\lambda_N = 12.0$ and $\lambda_L/\lambda_M = 28.0$. In this CS crossing, protons dominated: the $n_{H+}/n_{O+} = 2.0$, $n_{H+}/n_{O2+} = 4.0$, and $n_{H+}/n_{CO2+} = 22.0$ near the neutral plane of the CS. The ratio of the ion thermal pressure to the magnetic pressure is $\beta_{ION} = 15$ at the neutral plane. In this CS interval, ions also moved tailward with $V_X = -20$ and −10 km/s for protons and heavy ions, respectively (not shown).

Figure 3a′,b′ shows the spatial profiles of $B_L(l_N)$ and $J_M(l_N)$. Similarly to the previous example in this CS crossing, the slope of $B_L(l_N)$ changes near the neutral plane. The $J_M(l_N)$ profile can be fitted by two Harris layers with the current densities at the neutral plane: $J_{01} = 14$ nA/m^2 and $J_{02} = 4$ nA/m^2 and half-thicknesses $L_1 = 50$ km and $L_2 = 200$ km for the thin and thick current layers, respectively. The parameter of the embedding for this crossing $B_{L1}/B_0 = 0.28$ ($B_1 = 2.8$ nT and $B_0 = 10$ nT; see Figure 3a′). The absolute value of the magnetic field near the CS neutral plane $B_{CS} = 3$ nT.

In this CS configuration, protons become quasi-adiabatic ($\kappa < 1.0$) if their energies ≥10 eV. The gyroradius of 10 eV protons in the magnetic field outside the CS $B_0 = 10$ nT is $\rho_{H+} = 44$ km, which is of the order of the half-thickness of the thin current layer (L_1). Heavy ions become quasi-adiabatic already with energies of the order of a few eV. The gyroradius of 10 eV O^+ ions in the B_0 field is ~175 km, which is of the order of the half-thickness of the thick current layer (L_2).

Figure 3c′,d′ shows the hodograms of the magnetic field in the (B_N, B_L) and (B_M, B_L) planes, respectively. In this case, the B_N, component of the magnetic field at the neutral plane, is ~2.0 nT, and the intermediate-variance component $B_M = -2.5$ nT, so that $B_N/B_0 = 0.2$ and $|B_M|/B_0 = 0.25$. The comparison of the total ion current density J_{M_ION} at the neutral plane calculated as in the previous case (marked by a black cross in Figure 3b′) shows a good agreement with the maximum value of current density deduced from the magnetic field observations, J_{M_MF}.

2.2. Statistical Studies of the CS Characteristic Spatial Scales and Plasma Parameters

We apply the analysis similar to the one described in the previous section for the study of the CS crossings from our database (the list of the analyzed CS intervals is given in the Appendix). For all CSs from our database, the shear component of the magnetic field (B_M) was small at the neutral plane ($B_M/B_0 \leq 0.3$), while the normal component of the magnetic field in some CS intervals had a significant value $B_N/B_0 > 0.3$. Because the value of the magnetic field at the neutral plane influences the particle's adiabaticity (the parameter κ), one may expect the modulation of the CS structure with the B_N/B_0 increase.

To check this assumption, we divided the CS intervals from our database onto two groups with the $B_N/B_0 < 0.3$ and $B_N/B_0 \geq 0.3$. In Figure 4 we present several typical spatial profiles of the $B_L(l_N)$ (see Figure 4a,a′) and the corresponding profiles of the $J_M(l_N)$ (Figure 4b,b′) for each group of the CSs (the left and right columns in Figure 4). One can see that thin and intense current layers are observed only in the group with the $B_N/B_0 < 0.3$ (left column). These layers are embedded in thicker layers so that the parameter of embedding introduced in the previous section ranges for these CS intervals from ~0.25 to 0.65. In the CSs

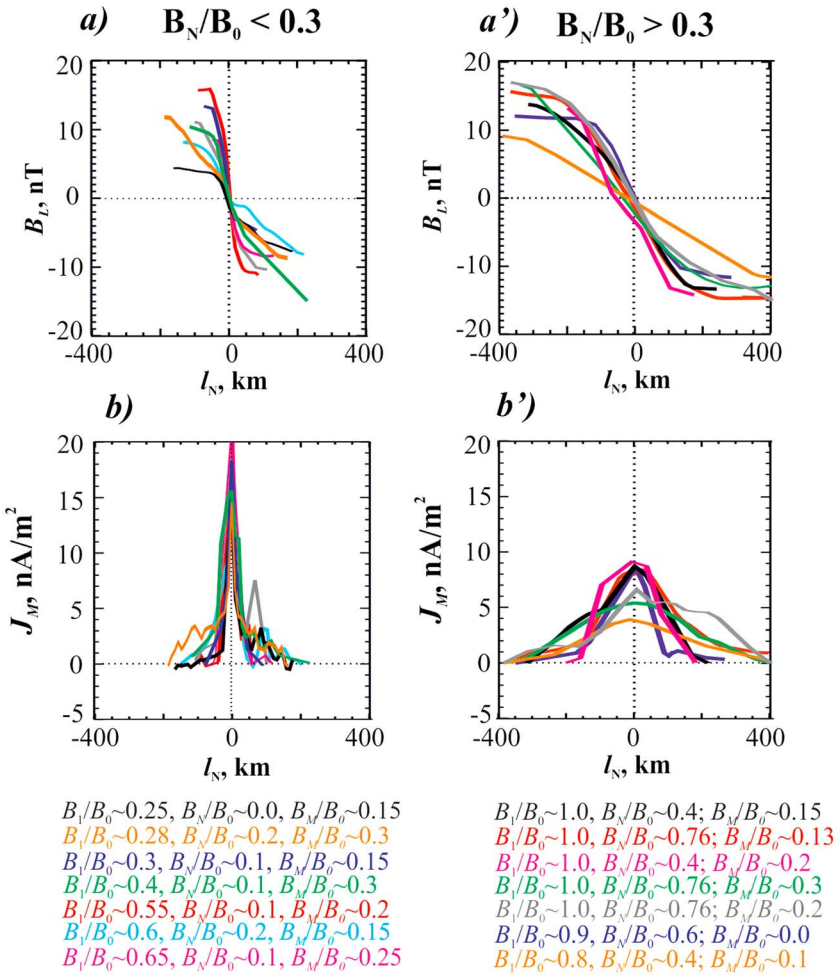

Figure 4. Several examples of the CS structures with small $B_N/B_0 < 0.3$ (the left column) and large $B_N/B_0 > 0.3$ (the right column). From top to bottom in each column: the spatial profiles of $B_L(l_N)$ (panels a, a′) and $J_M(l_N)$ (panels b, b′) are presented.

from the second group ($B_N/B_0 > 0.3$) the embedded thin layer disappears: the parameters of embedding approach 1.0, the thickness of the CS increases, and the current density decreases (see the right column in Figure 4 and the values of embedding B_1/B_0 in the legend in the right bottom part of the Figure).

Figure 5 shows the distributions of the CS observation probability versus n_{H+}/n_{CO2+} (a), n_{H+}/n_{O2+} (b), n_{H+}/n_{O+} (c), and ion β (d). The majority (~70%) of the CSs from our database are oxygen dominated with n_{H+}/n_{O2+} and $n_{H+}/n_{O+} < 1.0$, and carbon dioxide is a minor constituent in all CS intervals in our database ($n_{O2+} >> n_{CO2+}$, not shown). The majority of the CSs from our database have $\beta > 10.0$ at the neural plane.

Figure 6 presents the ratio of ion temperatures T_{H+}/T_{CO2+} (a), T_{H+}/T_{O2+} (b), and T_{H+}/T_{O+} (c) observed near the neutral plane of the CSs from our database. It is seen that in the majority of the CSs, heavy ions are hotter than protons. The similar situation takes place in the Earth's magnetotail, where due to the quasi-adiabatic interactions with the CS, heavy ions obtain larger energy gain than protons.

Figure 7 shows a scatterplot of the density of major ion components observed at the neutral plane of each CS from our database versus the corresponding ion temperature. Each dot at the plots represents a particular CS interval. The color of each dot displays the type of the dominating ion component in a given CS crossing, that is, the ion component that has the largest number density in the CS in comparison to the densities of the other ion components. Similarly to the Earth's plasma sheet in the Martian CSs, there is an inverse $n(T)$ dependence observed for each ion component: the colder ion populations in the CSs have larger densities and vice versa. The majority of the CSs from our database is dominated

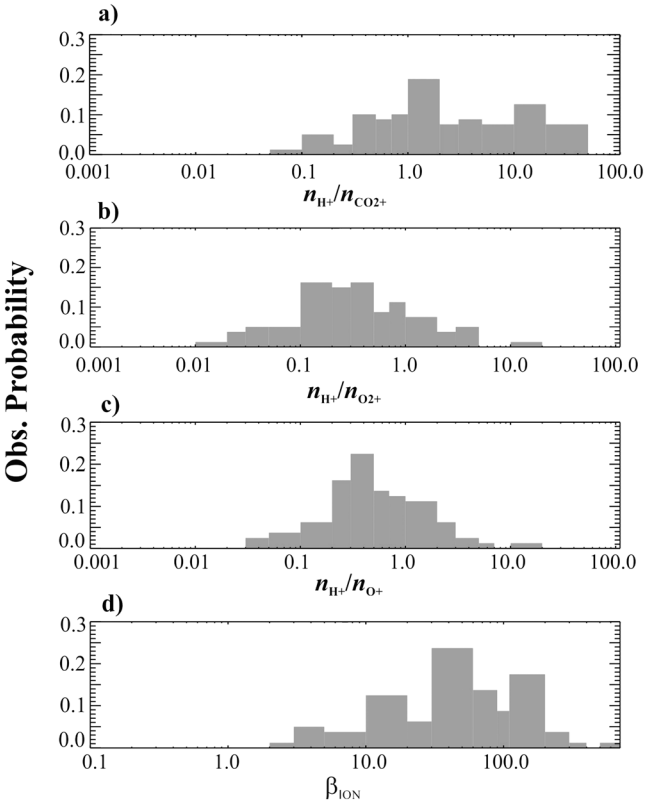

Figure 5. The histograms of the CS observation probability in dependence on the ratio of n_{H+}/n_{CO2+} (a); n_{H+}/n_{O2+} (b); n_{H+}/n_{O+} (c), and β_{ION} (d).

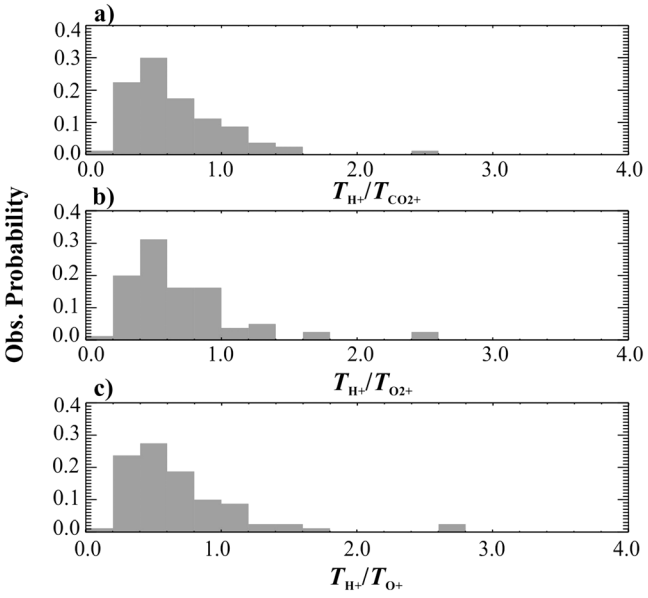

Figure 6. The histograms of the CS observation probability in dependence on the ratio of T_{H+}/T_{CO2+} (a); T_{H+}/T_{O2+} (b); and T_{H+}/T_{O+} (c).

by heavy ions (mostly by O_2^+ ions). The O_2^+-dominated CSs are shown by green dots, and many of them are characterized by low temperatures and high densities of all ion components. A few CSs from our database are relatively hot and tenuous: T_{H+} exceeds tens of eV, the temperatures of heavy ions exceed hundreds of eV, and ion densities are lower than 10.0 cm^{-3}.

In the Earth's plasma sheet, the observation of hot and tenuous plasma can be related with magnetic reconnection, which produces hot and underpopulated plasma flux tubes (e.g., Sharma et al., 2008, and references therein). The origin of similar plasma population in the Martian CS deserves a separate study.

3. Quasi-Adiabatic Modeling of the Martian CS

In this section, we model the formation of thin embedded CS structures in the Martian magnetotail and establish their scaling characteristics. To describe the CS in the Martian magnetotail, we modified the hybrid self-consistent model based on a quasi-adiabatic dynamics of oxygen ions and protons, which was developed for the modeling of thin CS in the Earth's magnetotail. The model takes into account two general magnetic components: the tangential to the CS plane (B_L) and the normal component (B_N). The B_L component is calculated in the frame of self-consistent calculations, while the B_N component is taken from MAVEN observations and is assumed to be constant in the CS. Basic principles of this model are described in papers by Zelenyi et al. (2004) and Zelenyi et al. (2006). The quasi-adiabatic model was developed under the following assumptions:

1. The CS is supported by plasma inflows from the northern and southern sources
2. The spatial scale of the CS along the normal direction (along N) is much smaller than its characteristic scales in the plane tangential to the CS, that is, in the (L, M) plane. Thus, all variables depend only on the coordinate N
3. The CS is considered in the deHoffmann-Teller coordinate system, where the electric field is absent
4. Plasma consists of magnetized electrons and three ion species: H^+, O^+, and O_2^+, which experience the quasi-adiabatic dynamics; that is, for these ion components, the parameter of adiabaticity $\kappa < 1.0$ (Büchner & Zelenyi, 1989), and the corresponding quasi-adiabatic invariant I_N (the analog of the first adiabatic invariant μ in the usual guiding center theory for $\kappa > 1.0$) is approximately conserved
5. The quasi-neutrality condition: $n_{O2+} + n_{O+} + n_{H+} = n_e$ is fulfilled

For such magnetic configuration, the Vlasov–Maxwell system of equations has the following form:

$$\frac{df_{1,2,3}(v,N)}{dN} = 0,$$

$$\frac{dB_L}{dN} = \frac{4\pi}{c}\left\{\int_{V^3} v_M\left[f_1(v,N) + f_2(v,N) + f_3(v,N)\right]d^3v + j_e(N,\varphi(N))\right\}d^3v$$

$$B_L(N)|_{N=L} = B_0, \varphi(N)|_{N=L} = 0$$

Here the index "1" refers to H^+ ions, the index "2" to O^+, and the index "3" to O_2^+ ions; $f_{1,2,3}$ are the velocity distribution functions of these ion components, B_0 is the magnetic field outside the CS (at $|N| = L$), $\varphi(N)$ is the electrostatic potential, j_e is the electron drift current, and v is the particle velocity. Because electrons are magnetized, they can be characterized by some average value of the magnetic moment μ, $p_{\|e}$, and $p_{\perp e}$ are correspondingly the

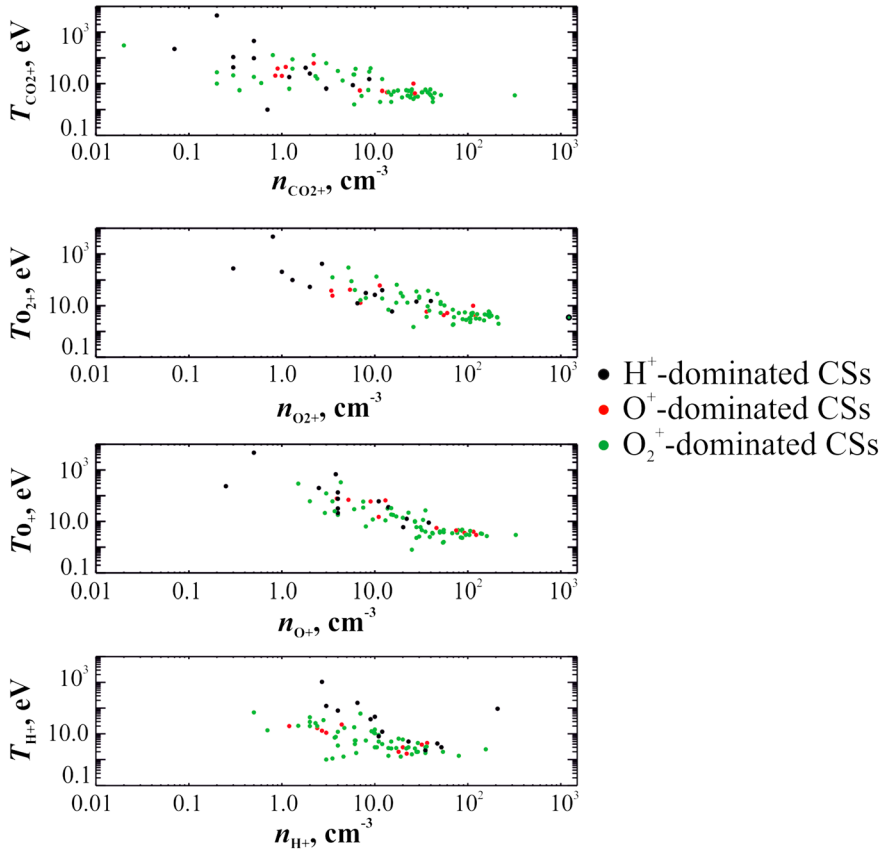

Figure 7. The scatterplots of temperature versus number density of a particular ion component observed at the neutral plane of each CS crossing from our database. The proton-dominated, O^+-dominated, and O_2^+-dominated CSs are displayed by the black, red, and green dots, respectively.

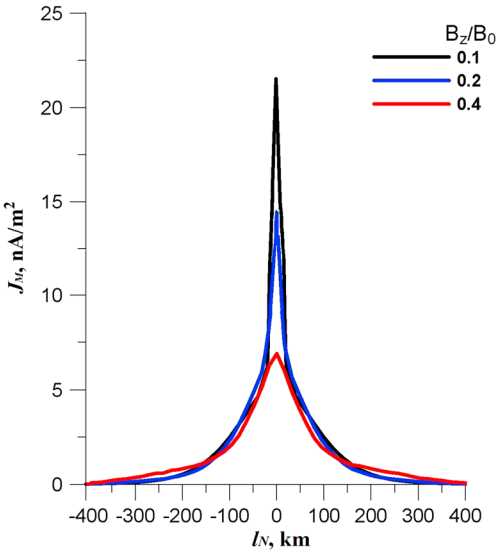

Figure 8. Three spatial profiles of the electric current density $J_M(l_N)$ obtained by the self-consistent quasi-adiabatic simulations for three different values of the normal component at the neutral plane: B_N/B_0 = 0.1, 0.2, 0.4 (shown by the black, blue, and red lines, respectively).

parallel and perpendicular components of their pressure tensor. Then the electron drift current has the following form:

$$j_e = -en_e c\frac{[E\times h]}{B} + \frac{c}{B}[h\times\nabla_\perp p_{\perp e}] + \frac{c}{B}(p_{||e} - p_{\perp e})[h\times(h\nabla)h] \quad (1)$$

where h = B/B. The detailed output of electrostatic potential and calculation of drift currents in the directions perpendicular and parallel to the magnetic field are given in Zelenyi et al. (2004; 2016). The distribution functions of proton and oxygen ion inflows at the edges of the CS are given in the form of the shifted Maxwell distribution: $f_{1,2,3}(v) = \exp[-(v_{||} \pm v_{D1,2,3})^2 + v_\perp^2]/v_{T1,2,3}^2]$. We used the relation between particle magnetic moments $\mu \equiv mv_\perp^2/2B_0$ and the quasi-adiabatic invariant IN outside the CS: μ = (e/2mc)lN (Sitnov et al., 2000), because they coincide in this region up to some normalization constant. Finally, one can rewrite the distribution function of the plasma sources in terms of invariants of motion $f_{1,2,3}(W_0, I_N)$, where W_0 is the total energy of the particles, and extrapolate these functions to the entire space using the Liouville's theorem (Zelenyi et al., 2004).

In contrast to the CSs of the Earth's magnetotail, the Martian CS are characterized by a wide range of ion densities and temperatures (see, e.g., Figure 7). Thus, to check if the quasi-adiabatic model can describe the main features of the Martian CS such as the embedding and the characteristic spatial scales, we used some average parameters observed by MAVEN:

B_N/B_0 = 0.1, 0.2, 0.4 (see three current density profiles in Figure 8); $n_{O+} = n_{O2+}$ and $n_{H+} = 0.1{\cdot}n_{O+}$; $\varepsilon_{H+} = \varepsilon_{O+} = \varepsilon_{O2+} = 0.3$ ($\varepsilon = V_T/V_D$, where V_T is the thermal velocity and V_D

is the drift velocity of a particular ion component outside the CS); the initial half-thickness of the CS is assumed to be ~ρ_{O2+} = 300 km (the thermal gyroradius of O_2^+ ions outside the CS). It was assumed that outside the CS the value of magnetic field is B_0 = 10 nT and plasma density n_0 = 10 cm^{-3}.

The system of Vlasov–Maxwell equations was solved numerically, and as a result, the self-consistent profiles of electric current density were found. Figure 8 shows the three spatial profiles of the current density $J_M(l_N)$ for three different values of the normal component at the neutral plane: B_N/B_0 = 0.1, 0.2, 0.4. It is seen from the figure that in the case of very small normal component (B_N/B_0 = 0.1, the black profile), the electron drift currents can be strong due to the strong curvature current (third term in (1)) that is inversely proportional to the radius of curvature of the magnetic field lines at the neutral plane, which is controlled by the B_N (Zelenyi et al., 2004). This current along with the proton current produces a narrow peak in the $J_M(l_N)$ with the characteristic half-thickness $L_1 \le \rho_{H+}$. The narrow and strong current layer (~23 nA/m^2) is embedded in a thicker layer with significantly smaller current density (~5 nA/m^2), which is produced by heavy ions (by O^+ and O_2^+) with $L_2 = \rho_{O2+}$.

With the B_N increase (B_N/B_0 = 0.2), the electric current density in a thin layer decreases (blue profile) due to the increase of the curvature of the magnetic field lines. For the larger B_N/B_0, the oxygen current becomes dominant, the thickness of the CS increases, and the embedding feature is smeared (see the red profile for B_N/B_0 = 0.4).

The characteristic scales of thin and thick current layers as well as the value of J_M depend on the relative number densities of the ion components, B_N/B_0, ion temperatures, and parameter ε. After using some average plasma parameters observed in the Martian CS, we can achieve a good agreement of the scales of model CS scales with the observed ones: L_1 = 40 km = ρ_{H+}, L_2 = 350 km = ρ_{O2+}; and the maximum current density J_M = 10–20 nA/m^2.

4. Discussion and Summary

The STATIC/MAVEN observations revealed a variety of ion composition and plasma parameters in the near-Martian CS observed at $-2.8\ R_M \le X_{MSO} \le -1.0\ R_M$. Below, we summarize the main characteristics of the CSs from our database:

1. The relative densities of light (H^+) and heavy ions (O^+, O_2^+, and CO_2^+) in the CSs from our database are in the following range:$0.04 \le n_{H+}/n_{O+} < 12.5$; $0.015 \le n_{H+}/n_{O2+} < 10.5$ and $0.08 \le n_{H+}/n_{CO2+} < 42.0$. The median values are $<n_{H+}/n_{O+}> = 0.4$; $<n_{H+}/n_{O2+}> = 0.3$, and $<n_{H+}/n_{CO2+}> = 1.4$
2. The ion temperatures range from a few electronvolts and up to a few kiloelectronvolts, and the ion number densities range from ~0.2 to ~300.0 cm^{-3}. The median values are $<T_{H+}>$ = 5 eV, $<T_{O+}> = <T_{O2+}> = <T_{CO2+}>$ = 9.5 eV, $<n_{H+}>$ = 10.0 cm^{-3}, $<n_{O+}>$ = 27.0 cm^{-3}, $<n_{O2+}>$ = 40.0 cm^{-3}, and $<n_{CO2+}>$ = 8.5 cm^{-3}. The ion number density in the CS is inversely proportional to the ion temperature (see Figure 7);
3. The ion β ranges from 2.0 to 623.0 at the neutral plane of the CS and the median value is $<\beta>$ = 58.5;
4. The ratios of light ion temperature to the temperature of heavy ions are $0.1 \le T_{H+}/T_{O+} < 9.5$; $0.1 \le T_{H+}/T_{O2+} < 14.0$ and $0.1 \le T_{H+}/T_{CO2+} < 13.5$, and the median values are $<T_{H+}/T_{O+}> = <T_{H+}/T_{O2+}> = <T_{H+}/T_{CO2+}> = 0.5$. Thus, in the majority of the CSs from our database, heavy ions are hotter than protons;
5. In all CSs from our database, the parameter of adiabaticity κ near the neutral plane was <1.0 for the thermal proton population, and it was $<<1.0$ for the thermal population of heavy ions;
6. The half-thickness L of the CS estimated as a spatial scale of the magnetic field reversal ranges from a few tens of kilometers up to a few hundreds of kilometers.

Thus, in contrast to the CSs observed in the Earth's magnetotail (e.g., Baumjohann et al., 1989), the CS in the Martian tail are mainly populated by heavy ions and are characterized by higher densities and lower ion temperatures. However, the structure of the Martian CS acquires the characteristic features similar to the ones observed in the Earth's CS. Namely, a thin current layer embedded in a thicker one is observed for all CS with the small normal component B_N at the neutral plane ($B_N/B_0 < 0.3$). A half-thickness of the thin layer is about tens of kilometers, which is of the order or less than the gyroradius of thermal protons outside the CS. The quantitative parameter of the embedding, B_1/B_0, for such CS ranges from ~0.25 to ~0.65. In the CSs with larger

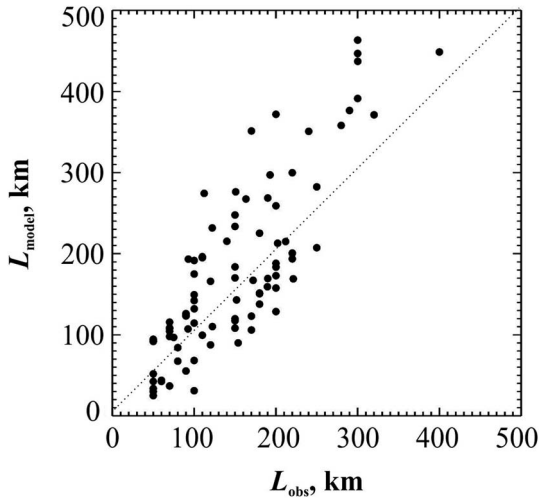

Figure 9. A scatterplot of the values of the CS half-thickness L_{model} estimated according to the model scaling law by using the magnetic and plasma parameters observed in each CS interval from our database versus the L_{obs} estimated for the corresponding CS as a spatial scale of the magnetic field reversal observed by MAVEN.

B_N ($B_N/B_0 > 0.3$), the embedding feature disappears (the parameter of embedding becomes ≥0.8), and the thickness of the CS increases, while the current density decreases (see Figure 4). For large B_N, the half-thickness of the CS is comparable with the gyroradius of the thermal O^+ or O_2^+ at the edge of the CS. The similar dependence of the CS structure on B_N was observed in the CSs of the Earth's magnetotail (e.g., Petrukovich et al., 2011).

The embedding features in the CS structure can be explained by the model of quasi-adiabatic ion dynamics (Zelenyi et al., 2006). This feature (and its quantitative characteristics B_1/B_0) depends on plasma characteristics in the CS. According to the quasi-adiabatic model developed for the Earth's magnetotail CS (Zelenyi et al., 2006), the embedding depends on the n_{O+}/n_{H+}, T_{O+}/T_{H+}, and the magnetic configuration of the CS. The increase of relative density of oxygen ions leads to the thickening of the CS and to the formation of oxygen current layer in the outer region of the CS. The density of oxygen current according to the author's estimate can reach ~30% of the maximum current density at the thin current layer. The increase of T_{O+}/T_{H+} provides a similar effect. The increase of $|B|$ at the neutral plane (due to the increase of the B_N and/or B_M components) results in the decrease of the amount of quasi-adiabatic particles and in the increase of their scattering that, in turn, leads to the decrease of the electric current density, CS expansion, and smearing of the embedding. These effects can be observed in the Martian CS. The quantitative analysis of the embedding and its dependence on the aforementioned parameters deserve a separate and careful investigation, which we plan to perform in our subsequent work.

In all CSs from our database, thermal ion populations experience quasi-adiabatic dynamics ($\kappa < 1.0$). To check the role of quasi-adiabatic ions in the formation of the Martian CS, we use the hybrid quasi-adiabatic model of the CS with three ion components: H^+, O^+, and O_2^+ with the plasma characteristics similar to the observed ones. The resulting self-consistent spatial profiles of the electric current density $J_M(I_N)$ have the structures very similar to the observed ones. For small B_N component at the neutral plane, a thin embedded current layer with L_1 = 40 km = ρ_{H+} is observed. The value of the model L_1 is close to the values of the estimated half-thickness of the thin CS from our database ~30–100 km. With the increase of the B_Z field, the embedded layer disappears and the CS expands. The half-thickness of the thick model CS L_2 = 350 km for B_N/B_0 = 0.4. For the CS from our database, the values of L_2 for $B_N/B_0 > 0.3$ range from 150 to 400 km (see Figure 4) and are comparable with thermal gyroradius of heavy ions (O^+ or O_2^+).

According to the theory of quasi-adiabatic ion dynamics, the half-thickness of the CS depends on the parameter $\varepsilon = V_T/V_D$ (here V_T is the thermal ion velocity in the CS and V_D is the drift velocity outside the CS), which characterizes the anisotropy of initial ion velocity distribution function (Zelenyi et al., 2000). The maximum value of $L = \rho_T$ (ρ_T is the thermal gyroradius of ions at the edges of the CS) is achieved in the case of weak plasma anisotropy ($\varepsilon \geq 1.0$). For larger anisotropy ($\varepsilon < 1.0$), there are two regimes: the quasi-adiabatic one, when $\varepsilon > B_N/B_0$ and the half-thickness of the CS $L = \rho_T\varepsilon^{1/3}$ and the regime of very strong anisotropy when $\varepsilon \leq B_N/B_0$ and the $L = \rho_T \cdot (B_N/B_0)^{4/3}$ (Zelenyi et al., 2000).

We check this scaling for the CSs from our database. For each CS crossing, the parameters ε and ρ_T were calculated for the dominant ion component in a given CS. The ρ_T was calculated by using the ion temperature and the magnetic field value observed at the edges of a particular CS. In Figure 9, we present a scatterplot of the L_{model} values calculated for each CS from our database according to the aforementioned theoretical scaling versus the L_{obs} value estimated for a given CS from MAVEN observations. There is more or less good agreement between the theoretical scaling and the observed values of the CS thickness. However, it is worth to note that the model overestimates the CS thickness for $L_{model} \geq 250$ km. For the majority of CSs in our database with $L_{obs} > 200$ km, the parameter ε is ≥1.0. According to the model, the thickness of such CS should be of the order of the thermal gyroradius of ions at the edges of the CS. To calculate the L_{model}, we used the gyroradius of dominating ion component (either O^+ or O_2^+ ions in the majority of cases). In such simple estimation, we did not take into account a fraction of lighter ions, which can decrease the CS thickness. This roughness provides some overestimated values of the model CS thickness in comparison with the observed ones.

Summarizing our results, we may conclude that in spite of the significant differences in the CS formation, ion composition, and plasma characteristics in the Earth's and Martian magnetotails, similar kinetic features are observed in the CS structures in the magnetotails of both planets. This phenomenon can be explained by the universal principles of nature. The CS once has been formed, then it should be self-consistently supported by the internal coupling of the total current carried by particles in the CS and its magnetic configuration, and as soon as the system achieved the quasi-equilibrium state, it "forgets" the mechanisms of its formation, and its following existence is ruled by the general principles of plasma kinetic described by Vlasov–Maxwell equations. The differences between the terrestrial and Martian CSs possibly can be seen in their 2D structure (i.e., their extents in the plane tangential to the CS plane can be different), but their 1D structure (along the normal to the CS plane) according to the general theoretical concepts should be similar. MAVEN observations discussed in this paper confirmed this expectation. In this paper we do not study the possible signatures of magnetic reconnection and its relation to the thin CSs observed in the Martian magnetotail. This important subject deserves a more detailed study, which we are going to make in future paper.

Appendix A

In Table A1, we list the CS intervals that we analyze in this paper along with the values of B_N/B_0 and B_{MID}/B_0 observed at the neutral plane.

Table A1
A List of the CS Intervals Analyzed in this Paper

Time interval, UT	Location in MSO (R_M)	$\lvert B_N/B_0\rvert$	$\lvert B_M/B_0\rvert$
1 December 2014 00:07:50–00:09:20	[−1.2, −0.3, 0.2]	0.13	0.06
1 December 2014 18:02:00–18:03:00	[−1.6, 0.3, −1.0]	0.12	0.05
1 December 2014 22:55:00–22:58:00	[−1.45, −0.1, −0.2]	0.06	0.12
2 December 2014 03:25:30–03:28:00	[−1.5, 0.1, −0.45]	0.0	0.0
2 December 2014 07:54:30–07:55:15	[−1.56, 0.2, −0.8]	0.0	0.1
2 December 2014 07:55:15–07:55:50	[−1.6, 0.2, −0.8]	0.75	0.18
2 December 2014 12:41:00–12:43:00	[−1.5, 0.0, −0.2]	0.12	0.17
2 December 2014 16:46:00–16:47:00	[−1.4, 0.6, −1.5]	0.6	0.1
2 December 2014 17:18:30–17:21:00	[−1.4, −0.1, −0.1]	0.27	0.14
3 December 2014 15:47:20–15:48:00	[−1.4, 0.6, −1.4]	0.0	0.17
3 December 2014 16:05:00–16:07:00	[−1.5, 0.2, −0.6]	0.0	0.2
3 December 2014 16:18:20–16:19:00	[−1.4, −0.1, 0.0]	0.53	0.11
3 December 2014 16:19:30–16:21:00	[−1.3, −0.1, 0.05]	0.08	0.08
4 December 2014 01:30:50–01:32:40	[−1.3, −0.1, 0.1]	0.25	0.25
4 December 2014 10:25:00–10:28:00	[−1.5, 0.3, −0.7]	0.12	0.12
4 December 2014 10:32:20–10:34:00	[−1.5, 0.1, −0.4]	0.0	0.05
4 December 2014 14:48:00–14:50:30	[−1.5, 0.5, −1.2]	0.0	0.15
5 December 2014 04:34:00–04:37:00	[−1.4, 0.6, −1.2]	0.0	0.23
5 December 2014 04:37:30–04:40:00	[−1.5, 0.5, −1.1]	0.0	0.28
5 December 2014 09:39:30–09:40:30	[−1.3, −0.1, 0.1]	0.1	0.12
5 December 2014 14:06:00–14:08:30	[−1.5, 0.1, −0.3]	0.15	0.15
6 December 2014 17:29:30–17:30:30	[−1.5, 0.4, −0.7]	0.06	0.27
6 December 2014 22:07:30–22:09:30	[−1.5, 0.3, −0.5]	0.09	0.18
7 December 2014 02:48:30–02:51:00	[−1.4, 0.1, −0.2]	0.0	0.12
7 December 2014 02:51:40–02:54:00	[−1.4, 0.1, −0.1]	0.16	0.22
7 December 2014 12:05:00–12:07:00	[−1.3, 0.0, 0.0]	0.18	0.0
8 December 2014 01:42:00–01:44:00	[−1.4, 0.2, −0.3]	0.0	0.25
8 December 2014 15:27:00–15:31:00	[−1.4, 0.2, −0.3]	0.11	0.07
8 December 2014 15:37:20–15:38:40	[−1.3, 0.0, 0.15]	0.32	0.0
8 December 2014 15:39:00–15:42:00	[−1.2, −0.1, 0.3]	0.12	0.25
9 December 2014 09:46:00–09:51:00	[−1.4, 0.3, −0.3]	0.0	0.12
9 December 2014 23:27:00–23:28:30	[−1.4, 0.2, −0.15]	0.0	0.2
10 December 2014 17:54:30–17:55:40	[−1.4, 0.3, −0.2]	0.16	0.0
11 December 2014 02:34:00–02:35:00	[−1.1, 1.0, −1.5]	0.05	0.2
11 December 2014 02:36:00–02:37:00	[−1.2, 1.0, −1.5]	0.08	0.16

Table A1. *(continued)*

Time interval, UT	Location in MSO (R_M)	$\lvert B_N/B_0 \rvert$	$\lvert B_M/B_0 \rvert$
11 December 2014 07:37:20–07:40:00	[−1.4, 0.3, −0.3]	0.2	0.2
11 December 2014 12:24:30–12:27:00	[−1.1, 0.0, 0.3]	0.2	0.06
11 December 2014 16:49:00 - 16:52:15	[−1.4, 0.3, −0.2]	0.3	0.2
11 December 2014 21:20:00–21:21:15	[−1.4, 0.4, −0.5]	0.07	0.07
11 December 2014 21:22:00–21:26:00	[−1.4, 0.3, −0.3]	0.03	0.06
12 December 2014 01:26:45–01:27:30	[−1.0, 1.0, −1.6]	0.1	0.1
12 December 2014 06:31:20–06:34:00	[−1.4, 0.4, −0.4]	0.32	0.12
12 December 2014 20:27:00–20:29:10	[−1.2, 0.1, 0.2]	0.26	0.13
13 December 2014 00:46:30–00:49:00	[−1.4, 0.5,-0.6]	0.1	0.27
13 December 2014 00:54:30–00:55:30	[−1.4, 0.3, −0.25]	0.0	0.1
13 December 2014 00:55:35–00:58:25	[−1.3, 0.3, −0.15]	0.12	0.29
14 December 2014 13:40:35–13:42:35	[−1.3, 0.2, 0.0]	0.1	0.27
15 December 2014 03:23:10–03:23:30	[−1.3, 0.3, −0.1]	0.0	0.1
15 December 2014 07:55:30–07:57:00	[−1.3, 0.35, −0.2]	0.12	0.28
15 December 2014 12:22:00–12:28:00	[−1.3, 0.5, −0.5]	0.1	0.2
15 December 2014 17:14:00–17:15:30	[−1.1, 0.0, 0.3]	0.12	0.12
15 December 2014 21:40:00–21:42:30	[−1.3, 0.35, −0.15]	0.33	0.1
17 December 2014 10:21:30–10:24:00	[−1.3, 0.3, 0.0]	0.43	0.28
18 December 2014 13:41:00–13:42:30	[−1.3, 0.7, −0.6]	0.3	0.29
18 December 2014 13:42:20–13:47:00	[−1.3, 0.6, −0.5]	0.2	0.29
18 December 2014 18:28:00–18:30:30	[−1.2, 0.3, 0.0]	0.15	0.25
20 December 2014 11:38:30–11:39:30	[−1.2, 0.5, −0.2]	0.18	0.27
20 December 2014 20:57:30–21:00:40	[−1.1, 0.1, 0.4]	0.25	0.25
21 December 2014 01:25:00–01:30:00	[−1.2, 0.3, 0.1]	0.4	0.1
23 December 2014 17:43:00–17:45:00	[−1.0, 0.1, 0.4]	0.26	0.26
24 December 2014 02:37:30–02:39:30	[−1.2, 0.7, −0.3]	0.2	0.2
24 December 2014 02:43:00–02:44:00	[−1.2, 0.5, 0.0]	0.0	0.14
24 December 2014 02:52:00–02:53:30	[−1.0, 0.2, 0.35]	0.0	0.27
24 December 2014 07:10:00–07:13:00	[−1.15, 0.6, 0.0]	0.2	0.29
27 December 2014 04:01:30–04:03:30	[−1.1, 0.6, 0.0]	0.1	0.29
29 December 2014 06:30:00–06:31:30	[−1.0, 0.4, 0.3]	0.14	0.14
29 December 2014 10:56:00–10:58:00	[−1.1, 0.8, −0.2]	0.2	0.0
29 December 2014 20:14:00–20:17:00	[−1.0, 0.4, 0.25]	0.33	0.1
31 December 2014 04:05:00–04:06:15	[−1.0, 1.0, −0.45]	0.0	0.25
31 December 2014 04:10:00–04:12:00	[−1.0, 0.8, −0.2]	0.12	0.29
31 December 2014 17:50:00–17:54:30	[−1.0, 0.9, −0.3]	0.25	0.15
2 April 2015 02:07:30–02:08:40	[−2.5, −1.2, −0.4]	0.0	0.14
2 April 2015 06:00:30–06:01:30	[−2.4, −0.5, 0.4]	0.14	0.0
2 April 2015 10:56:00–11:02:00	[−2.5, −1.0, −0.15]	0.14	0.14
3 April 2015 00:18:00–00:21:00	[−2.6, −0.7, 0.1]	0.1	0.27
3 April 2015 09:04:30–09:06:00	[−2.4, −0.35, 0.5]	0.0	0.17
16 April 2015 05:17:00–05:20:00	[−2.6, −0.6, −0.75]	0.0	0.28
16 April 2015 08:43:30–08:44:30	[−2.4, 0.5, 0.6]	0.2	0.0
16 April 2015 14:10:00–14:18:00	[−2.7, −0.5, −0.6]	0.12	0.25
17 April 2015 21:22:00–21:28:00	[−2.8, −0.1, −0.2]	0.14	0.2

Acknowledgments

We acknowledge NASA Planetary Data System (PDS) (http://atmos.nmsu.edu/data_and_services/atmospheres_data/MAVEN/maven_main.html), PI, and team of MAVEN spacecraft for the data access. We especially thank the efforts of the magnetometer group at GSFC in the design and implementation of the magnetometer investigation and the team of STATIC instrument for the prompt delivery of the data to the PDS. The MAVEN data used in this study were downloaded from the NASA PDS at http://atmos.nmsu.edu/data_and_services/atmospheres_data/MAVEN/maven_main.html. To obtain the data from a particular instrument, one should go to the instrument's homepage and download the calibrated data files. We thank Prof. O. L. Vaisberg for useful comments. The work of E. E. Grigorenko, S. D. Shuvalov, H. V. Malova, V. Yu. Popov, and L. M. Zelenyi is supported by the Russian Science Foundation (grant Nr. 16-42-01103). E. Dubinin acknowledges the support from DFG and DLR by grants PA 525/14-1 and 50QM1302, respectively.

References

Acuña, M. H., Connerney, J. E., Ness, N. F., Lin, R. P., Mitchell, D., Carlson, C. W., … Cloutier, P. (1999). Global distribution of crustal magnetization discovered by the Mars Global Surveyor MAG/ER experiment. *Science*, *284*, 790–793.

Acuña, M. H., Connerney, J. E. P., Wasilewski, P., Lin, R. P., Anderson, K. A., Carlson, C. W., … Ness, N. F. (1998). Magnetic field and plasma observations at Mars: Initial results of the Mars global surveyor mission. *Science*, *279*, 1676–1680. https://doi.org/10.1126/Science.279.5357.1676

Asano, Y., Mukai, T., Hoshino, M., Saito, Y., Hayakawa, H., Nagai, T. (2003). Evolution of the thin current sheet in a substorm observed by Geotail, *Journal of Geophysical Research*, *108*(A5), 1189, https://doi.org/10.1029/2002JA009785

Ashour-Abdalla, M., Zelenyi, L. M., Peroomian, V., & Richard, R. L. (1994). Consequences of magnetotail ion dynamics. *Journal of Geophysical Research*, *99*(A8), 14,891–14,916. https://doi.org/10.1029/94JA00141

Barabash, S., Fedorov, A., Lundin, R., & Sauvaud, J.-A. (2007). Martian atmospheric erosion rates. *Science*, *315*, 501–503. https://doi.org/10.1126/ science.1134358

Baumjohann, W., Blanc, M., Fedorov, A., & Glassmeier, K.-H. (2010). Current systems in planetary magnetospheres and ionospheres. *Space Science Reviews*, *152*(1–4), 99–134.

Baumjohann, W., Paschmann, G., & Cattell, C. A. (1989). Average plasma properties in the central plasma sheet. *Journal of Geophysical Research*, *94*, 6597–6606. https://doi.org/10.1029/JA094iA06p06597

Baumjohann, W., Paschmann, G., & Nagai, T. (1992). Thinning and expansion of the plasma sheet. *Journal of Goophysical Research*, *97*, 17,173–17,175. https://doi.org/10.1029/92JA01519

Baumjohann, W., Roux, A., Le Contel, O., Nakamura, R., Birn, J., Hoshino, M., … Runov, A. (2007). Dynamics of thin current sheets: Cluster observations. *Annales de Geophysique*, *25*, 1365–1389.

Bertucci, C., Duru, F., Edberg, N., Fraenz, M., Martinecz, C., Szego, K., & Vaisberg, O. (2011). The induced magnetospheres of Mars, Venus, and Titan. *Space Science Reviews*, *162*, 113–171. https://doi.org/10.1007/s11214-011-9845-1

Birn, J. (1987). Magnetotail equilibrium theory: The general three-dimensional solution. *Journal of Geophysical Research*, *92*, A10, 11,101–11,108.

Büchner, J., & Zelenyi, L. M. (1989). Regular and chaotic charged particle motion in magnetotaillike field reversals: 1. Basic theory of trapped motion. *Journal of Geophysical Research*, *94*(10), 11,821–11,842. https://doi.org/10.1029/JA094iA09p11821

Bunce, E. J., Cowley, S. W. H., & Wild, J. A. (2003). Azimuthal magnetic fields in Saturn's magnetosphere: Effects associated with plasma sub-corotation and the magnetopause-tail current system. *Annales Geophysicae*, *21*(8), 1709–1722.

Carlsson, E., Fedorov, A., Barabash, S., Budnik, E., Grigoriev, A., Gunell, H., … Dierker, C. (2006). Mass composition of the escaping plasma at Mars. *Icarus*, *182*, 320–328.

Connerney, J. E. P., Acuña, M. H., Ness, N. F., Kletetschka, G., Mitchell, D. L., Lin, R. P., & Reme, H. (2005). Tectonic implications of Mars crustal magnetism. *Proceedings of the National Academy of Sciences of the United States of America*, *102*(42), 14,970–14,975. https://doi.org/10.1073/pnas.0507469102

Connerney, J., Espley, J., Lawton, P., Murphy, S., Odom, J., Oliversen, R., & Sheppard, D. (2014). The MAVEN magnetic field investigation. *Space Science Reviews*, 1–35. https://doi.org/10.1007/s11214-015-0169-4

Crider, D. H., Brain, D. A., Acuña, M. H., Vignes, D., Mazelle, C., & Bertucci, C. (2004). Mars Global Surveyor observations of solar wind magnetic field draping around Mars. *Space Science Reviews*, *111*, 203–221. https://doi.org/10.1023/B:SPAC.0000032714.66124.4e

DiBraccio, G. A., Dann, J., Espley, J. R., Gruesbeck, J. R., Soobiah, Y., Connerney, J. E. P., … Jakosky, B. M. (2017). MAVEN observations of tail current sheet flapping at Mars. *Journal of Geophysical Research: Space Physics*, *122*, 4308–4324. https://doi.org/10.1002/2016JA023488

DiBraccio, G. A., Espley, J. R., Gruesbeck, J. R., Connerney, J. E. P., Brain, D. A., Halekas, J. S., … Jakosky, B. M. (2015). Magnetotail dynamics at Mars: Initial MAVEN observations. *Geophysical Research Letters*, *42*, 8828–8837. https://doi.org/10.1002/2015GL065248

Dubinin, E., & Fraenz, M. (2015). Magnetotails of Mars and Venus. In A. Keiling, C. M. Jackman, & P. A. Delamere (Eds.), *Magnetotails in the solar system* (pp. 43–59). Hoboken, NJ: John Wiley. https://doi.org/10.1002/9781118842324.ch3

Dubinin, E., Fraenz, M., Fedorov, A., Lundin, R., Edberg, N., Duru, F., & Vaisberg, O. (2011). Ion energization and escape on Mars and Venus. *Space Science Reviews*, *162*, 173–211. https://doi.org/10.1007/s11214-011-9831-7

Dubinin, E., Fraenz, M., Woch, J., Zhang, T. L., Wei, J., Fedorov, A., … Lundin, R. (2012). Bursty escape fluxes in plasma sheets of Mars and Venus. *Geophysical Research Letters*, *39*, L01104. https://doi.org/10.1029/2011GL049883

Dubinin, E., Lundin, R., Fränz, M., Woch, J., Barabash, S., Fedorov, A., … Carter, M. (2006). Electric fields within the Martian magnetosphere and ion extraction: ASPERA-3 observations. *Icarus*, *182*, 337–342. https://doi.org/10.1016/j.icarus.2005.05.022

Dubinin, E., Lundin, R., Norberg, O., & Pissarenko, N. (1993). Ion acceleration in the Martian tail: Phobos observations. *Journal of Geophysical Research*, *98*(A3), 3991–3997. https://doi.org/10.1029/92JA02233

Dubinin, E., Lundin, R., Riedler, W., Schwingenschuh, K., Luhmann, J. G., Russell, C. T., & Brace, L. H. (1991). Comparison of observed plasma and magnetic field structures in the wakes of Mars and Venus. *Journal of Geophysical Research*, *96*, 11,189–11,197. https://doi.org/10.1029/91JA01102

Eastwood, J. P., Brain, D. A., Halekas, J. S., Drake, J. F., Phan, T. D., Øieroset, M., … Acuña, M. (2008). Evidence for collisionless magnetic reconnection at Mars. *Geophysical Research Letters*, *35*, L02106. https://doi.org/10.1029/2007GL032289

Eastwood, J. W. (1972). Consistency of fields and particle motionin the 'Speiser' model of the current sheet. *Planetary and Space Science*, *20*, 10, 1555–1568.

Fedorov, A., Budnik, E., Sauvaud, J.-A., Mazelle, C., Barabash, S., Lundin, R., … Dierker, C. (2006). Structure of the Martian wake. *Icarus*, *182*, 329–336. https://doi.org/10.1016/j.icarus.2005.09.021

Fedorov, A., Ferrier, C., Sauvaud, J. A., Barabash, S., Zhang, T. L., Mazelle, C., … Bochsler, P. (2008). Comparative analysis of Venus and Mars magnetotails. *Planetary and Space Science*, *56*, 812–817. https://doi.org/10.1016/j.pss.2007.12.012

Ferguson, B. B., Cain, J. C., Crider, D. H., Brain, D. A., & Harnett, E. M. (2005). External fields on the nightside of Mars at Mars Global Surveyor mapping altitudes. *Geophysical Research Letters*, *32*, L16105. https://doi.org/10.1029/ 2004GL021964

Grigorenko, E. E., Malova, H. V., Artemyev, A. V., Mingalev, O. V., Kronberg, E. A., Koleva, R., … Zelenyi, L. M. (2013). Current sheet structure and kinetic properties of plasma flows during a near-Earth magnetic reconnection under the presence of a guide field. *Journal of Geophysical Research*, *118*, 3265–3287. https://doi.org/10.1002/jgra.50310

Grigorenko, E. E., Malova, H. V., Malykhin, A. Y., & Zelenyi, L. M. (2015). A possible mechanism of the enhancement and maintenance of the shear magnetic field component in the current sheet of the Earth magnetotail component. *Plasma Physics Reports*, *41*(1), 88–100.

Grigorenko, E. E., Zelenyi, L. M., Dolgonosov, M. S., Artemiev, A. V., Owen, C. J., Sauvaud, J.-A., … Hirai, M. (2011). Non-adiabatic ion acceleration in the Earth magnetotail and its various manifestations in the plasma sheet boundary layer. *Space Science Reviews*, *164*(1), 133–181. https://doi.org/10.1007/s11214-011-9858-9

Halekas, J. S., Brain, D. A., Lillis, R. J., Fillingim, M. O., Mitchell, D. L., & Lin, R. P. (2006). Current sheets at low altitudes in the Martian magnetotail. *Geophysical Research Letters*, *33*, L13101. https://doi.org/10.1029/2006GL026229

Halekas, J. S., Eastwood, J. P., Brain, D. A., Phan, T. D., Øieroset, M., & Lin, R. P. (2009). In situ observations of reconnection Hall magnetic fields at Mars: Evidence for ion diffusion region encounters. *Journal of Geophysical Research*, *114*, A11204. https://doi.org/10.1029/2009JA014544

Hara, T., Harada, Y., Mitchell, D. L., DiBraccio, G. A., Espley, J. R., Brain, D. A., … Jakosky, B. M. (2017). On the origins of magnetic flux ropes in near-Mars magnetotail current sheets. *Geophysical Research Letters*, *44*, 7653–7662. https://doi.org/10.1002/2017GL073754

Harada, Y., Halekas, J. S., McFadden, J. P., Mitchell, D. L., Mazelle, C., Connerney, J. E. P., … Jakosky, B. M. (2015a). Magnetic reconnection in the near-Mars magnetotail: MAVEN observations. *Geophysical Research Letters*, *42*, 8838–8845. https://doi.org/10.1002/2015GL065004

Harada, Y., Halekas, J. S., McFadden, J. P., Mitchell, D. L., Mazelle, C., Connerney, J. E. P., … Jakosky, B. M. (2015b). Marsward and tailward ions in the near-Mars magnetotail: MAVEN observations. *Geophysical Research Letters*, *42*, 8925–8932. https://doi.org/10.1002/2015GL065005

Harris, E. G. (1962). On a plasma sheet separating regions of oppositely directed magnetic field. *Nuovo Cimento*, *23*, 115–123.

Jakosky, B. M., Lin, R. P., Grebowsky, J. M., Luhmann, J. G., Mitchell, D. F., Beutelschies, G., … Zurek, R. (2015). The Mars Atmosphere and Volatile Evolution (MAVEN) Mission. *Space Science Reviews*, *195*, 3–48.

Kan, J. R. (1973). On the structure of the magnetotail current sheet. *Journal of Geophysical Research*, *78*, 19, 3773–3781.

Luhmann, J. G., & Brace, L. H. (1991). Near-Mars space. *Reviews of Geophysics*, *29*, 121–140.
Luhmann, J. G., Dong, C., Ma, Y., Curry, S. M., Mitchell, D. F., Espley, J., … Mazelle, C. (2015). Implications of MAVEN Mars near-wake measurements and models. *Geophysical Research Letters*, *42*, 9087–9094. https://doi.org/10.1002/2015GL066122
Luhmann, J. G., Russell, C. T., Schingenschuh, K., & Yeroshenko, Y. (1991). A comparison of induced magnetotails of planetary bodies: Venus, Mars, and Titan. *Journal of Geophysical Research*, *96*, 11,199–11,208. https://doi.org/10.1029/91JA00086
Lundin, R., & Barabash, S. (2004). The wakes and magnetotails of Mars and Venus. *Advances in Space Research*, *33*, 1945–1955. https://doi.org/10.1016/j.asr.2003.07.054
Lundin, R., Hultqvist, B., Olsen, S., Pellinen, R., Liede, I., Zakharov, A., … Pissarenko, N. (1989). The ASPERA experiment in the Soviet Phobos spacecraft. In J. H. Waite & T. E. Moore (Eds.), *Solar system plasma physics*, *Geophysical Monograph Series* (Vol. 54, pp. 417–424). Washington, DC: American Geophysical Union.
Lundin, R., Winningham, D., Barabash, S., Frahm, R. A., Andersson, H., Holmström, M., … Bochsler, P. (2006). Ionospheric plasma acceleration at Mars: ASPERA-3 results. *Icarus*, *182*, 308–319. https://doi.org/10.1016/j.icarus.2005.10.035
Lundin, R., Zakharov, A., Pellinen, R., Borg, H., Hultqvist, B., Pissarenko, N., … Koskinen, H. (1990). Plasma composition measurements of Martian magnetosphere morphology. *Geophysical Research Letters*, *17*, 877–880. https://doi.org/10.1029/GL017i006p00877
Malova, H. V., Popov, V. Y., Grigorenko, E. E., Petrukovich, A. A., Delcourt, D., Sharma, A. S., … Zelenyi, L. M. (2017). Evidence for quasi-adiabatic motion of charged particles in strong current sheets in the solar wind. *The Astronomical Journal*, *834*, 34. https://doi.org/10.3847/1538-4357/834/1/34
McFadden, J., Kortmann, O., Curtis, D., Dalton, G., Johnson, G., Abiad, R., … Jakosky, B. (2014). MAVEN suprathermal and thermal ion composition (STATIC) instrument. *Space Science Reviews*, *195*, 199–256.
Nagy, A., Winterhalter, D., Sauer, K., Cravens, T. E., Brecht, S., Mazelle, C., … Trotignon, J. G. (2004). The plasma environment of Mars. In D. Winterhalter, M. Acuna, & A. Zakharov (Eds.), *Mars' magnetism and its interaction with the solar wind* (pp. 33–114). Netherlands: Springer.
Nakamura, R., Baumjohann, W., Runov, A., & Asano, Y. (2006). Thin current sheets in the magnetotail observed by Cluster. *Space Science Reviews*, *122*, 29–38.
Petrukovich, A. A., Artemyev, A. V., Malova, H. V., Popov, V. Y., Nakamura, R., & Zelenyi, L. M. (2011). Embedded current sheets in the Earth's magnetotail. *Journal of Geophysical Research*, *116*, A00125. https://doi.org/10.1029/2010JA015749
Romanelli, N., Bertucci, C., Gómez, D., & Mazelle, C. (2015). Dependence of the location of the Martian magnetic lobes on the interplanetary magnetic field direction: Observations from Mars Global Surveyor. *Journal of Geophysical Research: Space Physics*, *120*, 7737–7747. https://doi.org/10.1002/2015JA021359
Runov, A., Baumjohann, W., Nakamura, R., Sergeev, V. A., Amm, O., Frey, H., … Klecker, B. (2008). Observations of an active thin current sheet. *Journal of Geophysical Research*, *113*, A07S27. https://doi.org/10.1029/2007JA012685
Runov, A., Nakamura, R., W. Baumjohann, Zhang, T.L., Volwerk, M., Eichelberger, H.-U., Balogh, A. (2003). Cluster observations of a bifurcated current sheet, *Geophysical Research Letters*, *30*2, 1036. https://doi.org/10.1029/2002GL016136.
Sergeev, V. A., Runov, A., Baumjohann, W., Nakamura, R., Zhang, T. L., Volwerk, M., … Klecker, B. (2003). Current sheet flapping motion and structure observed by Cluster, *Geophysical Research Letters*, *30*(6), 1327. https://doi.org/10.1029/2002GL016500.
Sharma, S., Nakamura, R., Runov, A., Grigorenko, E. E., Hasegawa, H., Hoshino, M., … Snekvik, K. (2008). Transient and localized processes in the magnetotail: A review. *Annales Geophysicae*, *26*, 955–1006.
Shindler, K. (1974). A theory of the substorm mechanism. *Journal of Geophysical Research*, *79*, 19, 2803–2809.
Sitnov, M. I., Zelenyi, L. M., Malova, H. V., & Sharma, A. S. (2000). Thin current sheet embedded within a thicker plasma sheet: Self-consistent kinetic theory. *Journal of Geophysical Research*, *105*, 13,029–13,044. https://doi.org/10.1029/1999JA000431
Sönnerup, B.U.Ö., & M. Scheible (1998). *Analysis methods for multi-spacecraft data*, In G. Pashmann & P. W. Daly, *ISSI Scientific Report SR-001* (Chap. 8, p. 185). Bern, Noordwijk, Netherlands: ESA Publication Division.
Speiser, T. W. (1965). Particle trajectories in model current sheets: 1. Analytical solutions. *Journal of Geophysical Research*, *70*, 4219–4226. https://doi.org/10.1029/JZ070i017p04219
Uritsky, V. M., Slavin, J. A., Khazanov, G. V., Donovan, E. F., Boardsen, S. A., Anderson, B. J., & Korth, H. (2015). Kinetic-scale magnetic turbulence and finite Larmor radius effects at Mercury. *Journal of Geophysical Research*, *116*, A09236. https://doi.org/10.1029/2011JA016744
Vaisberg, O. L. (1992). The solar wind interaction with Mars: A review of results from early Soviet missions to Mars. In *Venus and Mars: Atmospheres, ionospheres and solar wind interactions* (Vol. 66, pp. 311–326). Washington, DC: American Geophysical Union.
Vasko, I. Y., Zelenyi, L. M., Artemyev, A. V., Petrukovich, A. A., Malova, H. V., Zhang, T. L., … Nakamura, R. (2014). The structure of the Venusian current sheet. *Planetary and Space Science*, *96*, 81–89.
Yeroshenko, Y., Riedler, W., Schwingenschuh, K., Luhmann, J. G., Ong, M., & Russell, C. T. (1990). The magnetotail of Mars: Phobos observations. *Geophysical Research Letters*, *17*, 885–888. https://doi.org/10.1029/GL017i006p00885
Zelenyi, L., Artemyev, A., Malova, H., & Popov, V. (2008). Marginal stability of thin current sheets in the Earth s magnetotail. *Journal of Atmospheric and Solar - Terrestrial Physics*, *70*, 325–333.
Zelenyi, L. M., Delcourt, D. C., Malova, H. V., Sharma, A. S. (2002). "Aging" of the magnetotail current sheets. *Geophysical Research Letters*, *29*12, 1608. https://doi.org/10.1029/2001GL013789.
Zelenyi, L. M., Malova, K. V., Artemyev, A. V., Popov, V. Y., & Petrukovich, A. A. (2011). Thin current sheets in collisionless plasma: Equilibrium structure, plasma instabilities, and particle acceleration. *Plasma Physics Reports*, *37*(2), 118–160.
Zelenyi, L. M., Malova, H. V., Grigorenko, E. E., & Popov, V. Y. (2016). Thin current sheets: From the work of Ginsburg and Syrovatskii to the present day. *Uspekhi Fizicheskikh Nauk*, *186*(11), 1153–1188.
Zelenyi, L. M., Malova, H. V., Popov, V. Y., Delcourt, D. C., Ganushkina, N. Y., & Sharma, A. S. (2006). "Matreshka" model of multilayered current sheet. *Geophysical Research Letters*, *33*, L05105. https://doi.org/10.1029/2005GL025117
Zelenyi, L. M., Malova, H. V., Popov, V. Y., Delcourt, D., & Sharma, A. S. (2004). Nonlinear equilibrium structure of thin currents sheets: Influence of electron pressure anisotropy. *Nonlinear Processes in Geophysics*, *11*(1), 1–9.
Zelenyi, L. M., Sitnov, M. I., Malova, H. V., & Sharma, A. S. (2000). Thin and superthin ion current sheets. Quasi-adiabatic and nonadiabatic models. *Nonlinear Processes in Geophysics*, *7*, 127–139.
Zhang, T.-L., Schwingenschuh, K., Russell, C. T., Luhmann, J. G., Rosenbauer, H., Verigin, M. I., & Kotova, G. (1994). The flaring of the Martian magnetotail observed by the Phobos 2 spacecraft. *Geophysical Research Letters*, *21*, 1121–1124. https://doi.org/10.1029/94GL01073